Localized Ectopic Expression of *Dpp* Receptors in a *Drosophila* Embryo

By A. D. Lander, Q. Nie, F. Y. M. Wan[*]*, and Y.-T. Zhang*[†]

Receptor-mediated bone morphogeneric protein (BMP) degradation has been seen to play an important role in allowing for the formation of relatively stable morphogen signaling patterns. To the extent that receptors act as a "sink" for BMPs, one would predict that the localized over-expression of signaling receptors would cause a net flux of freely diffusing BMPs toward the *ectopic*, i.e., abnormally high concentration, receptor site. One possible consequence would be a depression of BMP signaling in adjacent areas because less BMPs are now available for binding with the same normal concentration of receptors at the adjacent areas. However, recent experiments designed to examine this possible effect were inconclusive. In this paper, we investigate the possibility of depression of BMP signaling outside the area of elevated receptor level in a *Drosophila* embryo by modeling mathematically the basic biological processes at work in terms of a system of nonlinear reaction-diffusion equations with spatially varying (and possibly discontinuous) system properties. The steady-state signaling morphogen gradient is investigated by the method of matched asymptotic expansions and by numerical simulations.

[*]Address for correspondence: F. Y. M. Wan, University of California, Irvine, CA 92697-3875, USA; e-mail: fwan@uci.edu

[†]Y. T. Zhang is now an Assistant Professor at the University of Notre Dame.

STUDIES IN APPLIED MATHEMATICS 123:175–214

1. Introduction

For proper functioning of tissues and organs, cells are required to differentiate appropriately for its position. Positional information that instructs cells about their prospective fate is often conveyed by concentration gradients of morphogens, also known as (aka) ligands, bound to cell receptors (*bound-morphogens* for short). Morphogens/ligands are "signaling" protein molecules that, when bound to appropriate cell receptors, trigger the genetic program to assign/express different cell fates at different concentrations [1, 2]. Morphogen activities are of special importance in understanding the development of a population of uncommitted cells in an embryo to create complex patterns of gene expression in space. This role of morphogens has been the prevailing thought in tissue patterning for over half a century; but only recently have there been sufficient experimental data [1–4] and adequate analytical studies (see [5–8] and references therein) for us to begin to understand how various useful morphogen concentration gradients are formed.

Dorsal–ventral (belly-back) patterning in vertebrate and *Drosophila* embryos is now known to be regulated by bone morphogeneric proteins (BMP). The BMP activity is mainly controlled by several secreted factors including the antagonists chordin and short gastrulation (*Sog*). In *Drosophila* fruit flies, seven zygotic genes have been proposed to regulate dorsal–ventral patterning. Among them, decapentaplegic (*Dpp*) encodes BMP homologues that promotes dorsal cell fates such as amnioserosa and inhibits development of the ventral central nervous system. On the other hand, the chordin homologue *Sog* promotes the development of central nervous system.

Typically, morphogen concentration gradients are synthesized at certain part of the embryo, followed by their diffusion, binding with receptors (or other nonsignaling molecules known collectively as *nonreceptors*) and degradation in appropriate regions [7]. In the above *Dpp–Sog* system, the production of *Dpp* is pretty much uniform in the dorsal region and not at all in the ventral region while the opposite is true for *Sog*. The *Dpp* activity has been found to have a sharp peak around the midline of the dorsal in the presence of its "inhibitor" *Sog* (much more so during the transient phase than in steady state). Intriguingly, mutation of *Sog* results not only in a loss of ventral structure as expected, but the amnioserosa is reduced in addition. This result is paradoxical as the amnioserosa is the dorsal-most tissue and apparently a BMP antagonist is required for maximal BMP signaling [9–12].

As the system contains many variables, the question of what leads to a sharp (bounded) *Dpp* concentration peak is difficult to tackle by traditional experimental means. In [13], a quantitative analysis (along with experimental studies) of this phenomenon was undertaken by extending the *one-dimensional* dynamic *Dpp–Sog* system formulated in [14] and [15] for the evolution of the morphogen activities in the extracellular space with *Dpp* and *Sog* produced in

the dorsal and ventral regions, respectively, possibly at different prescribed production rates. The system allows for diffusion, reversible binding, and degradation of the two morphogens, *Dpp* and *Sog,* as well as reversible binding and degradation of *Dpp* bound to its signaling cell receptors Thickvein (*tkv*). The extension consists of allowing the enzyme *Tolloid* to cleave *Dpp–Sog* complexes to (degrade *Sog* and) free up *Dpp* molecules. Numerical simulations of this relatively simple model for the process of dorsal–ventral patterning in [13] were found to capture the Sog-dependent shuttling of BMPs to the dorsal midline and provide insights into the unusual dynamics of this gradient formation process.

In the model examined in [13], receptor-mediated BMP degradation plays an important role in allowing for the formation of relatively stable PMad patterns. To the extent that signaling receptors act as a "sink" for BMPs, one would predict that the localized over-expression of these receptors would cause a net flux of free BMPs toward the ectopic (abnormally high) receptor concentration site. One possible consequence would be a depression of BMP signaling in adjacent areas because less BMPs are now available for binding with the same concentration of receptors at the adjacent areas as before. Recently, Wang and Ferguson [16] presented experiments in which mRNA for the Dpp receptor *tkv* was injected in a localized fashion into early embryos. No discernible difference were observed in the patterns of morphogen signaling, i.e., phosphorylated Mad protein (PMad) patterns, that ultimately developed (unless a constitutively active form of the receptor was used).

The experiments of Wang and Ferguson were carried out by RNA injection; it is not possible to know whether the levels of ectopic *tkv* were substantial compared with endogenous *tkv* and therefore whether they should have been expected to have any significant influence on BMP degradation. To gain additional information on this issue, GAL4-UAS was used in [13] to express ectopic *tkv* in the head region of embryos and its subsequent effects on PMad staining observed. As shown in supplemental figure S7 of [13] (reproduced from the Supplement of [13] as Figure 1 below), endogenous *tkv* expression in the embryonic head region is already relatively substantial and can be elevated by expressing wild-type *tkv* using a bcd-GAL4 driver. When compared with wild-type embryos, those expressing ectopic *tkv* consistently showed a narrowing and weakening of the PMad staining pattern over a range of 10–12 cell diameters posterior to the border of the bcd domain. Thus, the data are consistent with the supposition on the model earlier that there would be a depression of BMP signaling outside the area of elevated *tkv*.

The experimental results of [13] notwithstanding, a closer examination of the biological processes at work suggests some uncertainty regarding the actual effects of a localized over-expression of *tkv.* Given that there is no shortage of free *Dpp* throughout the dorsal region of the embryo in steady state, there is no obvious necessity for a depression of bound-*Dpp* concentration outside

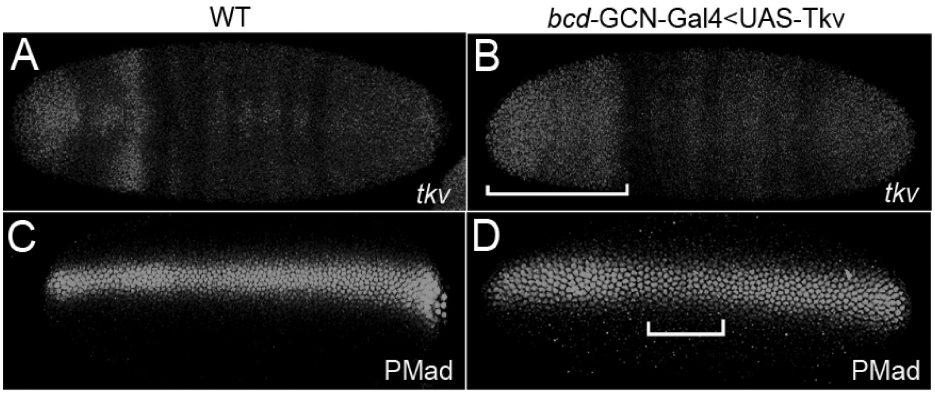

Figure 1. Localized expression of Tkv leads to reduced PMad activation in adjacent cells (reproduced from figure 7 of the SOM for [13]): (A) Endogenous *tkv* expression in a wild-type embryo. Note that expression is elevated in the sections of head relative to the trunk region. At this stage, *tkv* expression is restricted to the dorsal region of the embryo. Embryos are viewed from a dorsal perspective with anterior to the left in this and subsequent panels. (B) Over-expression of a UAS-*tkv* transgene in the head with the bcd-GCN4/GAL4 driver results in increased *tkv* expression in an anterior cone of cells that circumnavigates the entire D/V axis in the head region (bracket). The level of ectopic tkv expression in dorsal cells is approximately equal to that of endogenous *tkv*. (C) PMad staining in a wild-type embryo. (D) PMad staining in an embryo expressing tkv in the head under the control of the bcd-GCN4/GAL4 driver. Note that the width and level of PMad expression is decreased in trunk cells lying posterior to the domain of *tkv* over-expression. This depression of PMad staining extends for 10–12 cells. (Reprinted from Developmental Cell, Vol. 8, Claudia Mieko Mizutani, Qing Nie, Frederic Y.M. Wan, Yong-Tao Zhang, Peter Vilmos, Rui Sousa-Neves, Ethan Bier, J. Lawrence Marsh, Arthur D. Lander, Formation of the BMP Activity Gradient in the *Drosophila* Embryo, pp. 915–924, June 2005, with permission from Elsevier).

the area of elevated *tkv* even if some of the free *Dpp* has been siphoned off by the ectopic receptors. Furthermore, whether there should be a depression of BMP signaling may depend on the level of *Sog* synthesis rate given the *Sog*-dependent shuttling of BMPs to the dorsal midline. We investigate these issues herein by obtaining steady-state solutions of a relevant mathematical model for the biological development of interest.

The mathematical model of the aforementioned embryonic development is necessarily more complex than those previously analyzed by the authors in [7, 8, 13, 15] and references therein. Given the spatial variations of the synthesis rates of *Dpp* and *Sog* along the dorsal–ventral axis and the spatial variations of *tkv* concentration in the anterior–posterior direction, the model must be at least spatially two-dimensional. With *Dpp, Sog* and the *Dpp–Sog* complexes diffuse freely in the extracellular space, the model must be multi-diffusional even if we should take the diffusion rates to be (more or less) identical. In Section 2, the roughly cigar shape embryo is idealized and simplified to make our first analysis tractable. A two-dimensional extension of the extracellular

model used in [15] for this simplified domain turns out to be adequate for our purpose. The relevant initial-boundary value problem (IBVP) is formulated for the idealized problem. With the new mathematical problem similar to that treated in [15] except that it is now spatially two-dimensional, much of the theoretical development in [15] can be extended to assure the existence of a steady-state solution. We therefore focus on obtaining approximate solutions for the steady-state problem to gain insight to the steady-state behavior in the presence of ectopic receptor expression.

Similar to the simpler one-dimensional case of a uniform receptor expression treated in [15], the restriction of complete immobility of *Dpp* (as suggested by Eldar et al. [5]) is not required for the existence of a steady-state behavior for the present problem (see also [13]). For a sufficiently high *Sog* synthesis rate, we are able to obtain an outer (asymptotic expansion) steady-state solution with respect to the small Dpp-to-Sog synthesis rate ratio for our problem. More remarkably, the effects of ectopic receptor expression for this case can be obtained from the aforementioned outer solution alone without the rather complex inner solutions (and the attendant matching) required in a related problem in [17] or numerical simulations as in [18] to deal with the layer phenomena in the neighborhood of the various receptor concentration and synthesis rate discontinuities. Conditions under which there would be a depression of bound-*Dpp* concentration posterior to the elevated *tkv* area can then be analyzed. We also examine the relatively high *Dpp* synthesis rate case and show that a regular perturbation solution is sufficient for the determination of the effects of ectopic receptors. The intermediate case of comparable *Dpp* and *Sog* synthesis rates admits no useful simplifications and is investigated by accurate numerical simulations.

2. The mathematical model

2.1. Idealized geometry for the extracellular domain

Depending on the stage of development it is in, an embryo may be of different shapes. For the period of development of interest here, the embryo of a *Drosophila* fruit fly is typically somewhere between the shape of a football and a cigar and may be treated as a prolate spheroid (see Figure 2(A)) for the purpose of analysis. For an extracellular model, we are concerned mainly with biological activities on the surface of the embryo with the various concentration gradients being scalar fields defined on the surface of the prolate spheroid. While we can formulate the equations governing these concentration gradients in terms of the conventional prolate spheroidal coordinates with the z-axis along the length and through the center of the cross section (of the embryo), we simplify it substantially in our preliminary study of this problem by mapping the relevant part of the surface domain into a rectangle in the Cartesian plane.

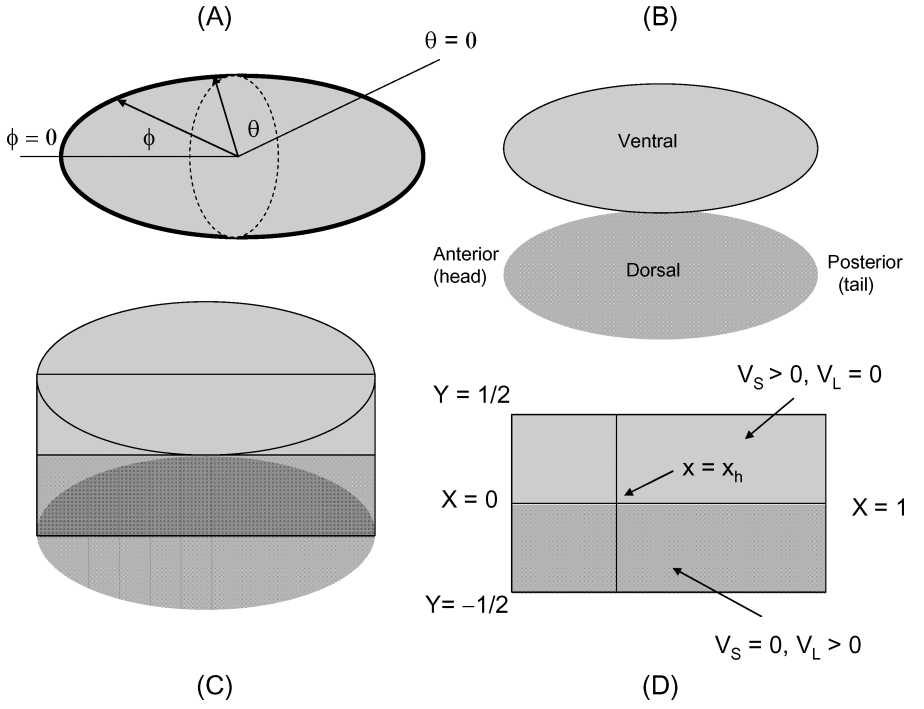

Figure 2. (A) Prolate spheroidal surface domain; (B) dorsal and ventral portion of prolate spheroidal surface; (C) half of the mirror-symmetric domain; (D) idealized half domain as a rectangle in the X- and Y-plane.

For our investigation, we imagine cutting the prolate spheroidal surface along the one continuous mid-line of both dorsal and ventral part of the embryo (see Figure 2 (B) and (C)). Given the symmetry of development activities with respect to the dorsal and ventral mid-line, we only need to consider one of the two half prolate spheroidal surfaces resulting from the fictitious cut. We further map the relevant half prolate spheroidal surface (consisting half of the dorsal region and the adjacent half of the ventral extending from the dorsal mid-line to the ventral mid-line) into the rectangular region Ω_{XY} in the X,Y-plane, which spans from $-Y_{\max}/4$ to $Y_{\max}/4$ in the polar direction and from 0 to $X_{\max}$ in the azimuthal direction. Note that $Y_{\max}$ is the circumference of the average cross section of the embryo with the z-axis of the prolate spheroidal coordinate system (which is parallel to the direction of the antero–posterior axis and the x-axis of the Cartesian rectangle Ω_{XY}) as its normal (see Figure 2(D)).

As indicated in the Figure 2(D), *Sog* is synthesized at a constant rate V_S and only in the ventral region while *Dpp* at a constant rate V_L only in the dorsal region. Both diffuse away from the respective localized source and bind with each other while *Dpp* also binds to signaling receptors *Thickvein* (*tkv*) which is attached to the cell membrane. Some of these

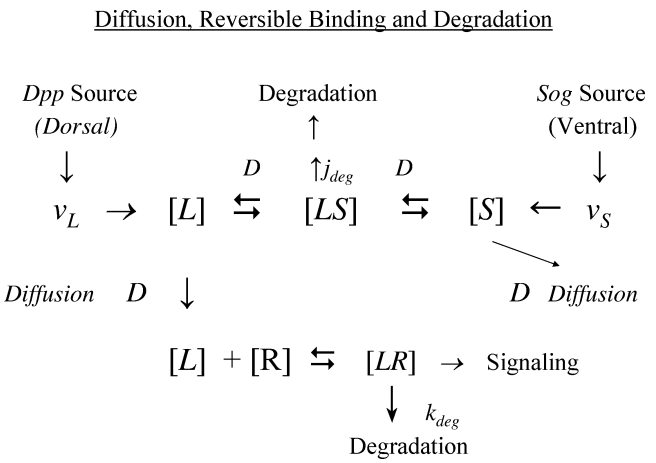

Figure 3. Schematic diagram of biological processes.

complexes will degrade while others dissociate to free up morphogens and receptors for new binding action. Generally, the receptors also degrade and new one generated at a rate V_R. The model in this paper does not have an explicit account for the synthesis, internalization (through endocytosis), and degradation of (free or bound) receptors. As System B in [7] and [19], we limit ourselves to the case of a fixed receptor concentration $R(X)$ corresponding to the case of a receptor synthesis rate matching its degradation rate with internalization implicit in receptor-mediated degradation. (An alternative and equally unrealistic interpretation would be that degradation of a *bound Dpp* complex destroys only the *Dpp* molecule and releases the receptor involved for binding with another free *Dpp* molecule.) The omission of an explicit account of receptor renewal and internalization in no way affects the usefulness of our analysis; we have already established in [19, 20] that the BVP governing the steady-state behavior of more general models which include receptor renewal and internalization can be reduced the corresponding BVP for the simpler fixed receptor system. The effects of the more general case of receptor renewal have also been examined and will be reported in a future publication.

2.2. The initial-boundary value problem

The allowable set of developmental activities of the two interacting morphogens *Dpp* and *Sog* in our idealized embryo is summarized schematically in Figure 3. For an analytical and computational study of the biological development of this idealized embryo, the essential features of the allowable activities are described mathematically by a system of partial differential equations (PDE) and auxiliary conditions [13]. This approach was first applied to study the development of the *Drosophila* wing imaginal disc [7, 21, 22]. The three basic biological processes

involving *Dpp* in the wing disc are the diffusion of free *Dpp* molecules, their reversible binding with renewable receptors, and degradation of the *Dpp*-receptor complexes (aka bound *Dpp*). The main purpose of [7, 22] was to investigate the role of diffusion in the formation of a *Dpp*-receptor concentration gradient in the wing disc. That system was extended to include the effect of *Sog* on the *Dpp* activity in a dorsal–ventral configuration [14] in an embryo with the cleavage of *Dpp–Sog* complexes by *Tolloid* implicitly incorporated into the system through the complete recovery of *Dpp* after cleavage (while the Sog components degrade). The cleavage and recovery phenomenon has been suggested by previous experimental studies [23, 24]. An even more general system was investigated in [15] where we allowed fractional recovery (in an extracellular model) through the fraction parameter $\tau, 0 \leq \tau \leq 1$, with $\tau = 1$ corresponding to complete recovery.

The setting for dorsal–ventral patterning in a *Drosophila* embryo during development with localized over-expression of *tkv* receptors is different and more complex than those considered in [7, 8, 13, 15, 20, 25]. As shown in the sketch of the dorsal–ventral cross-section of the embryo in Figure 2, *Dpp* is only produced in the dorsal region (with the temporally uniform rate $V_L(X)$) while *Sog* is only produced in the ventral region (with the rate $V_S(X)$). With *tkv* over-expressed along only a part of anterior–posterior direction, the biological development of the embryo is no longer uniform in that direction as it was in the problem investigated in [15]. The appropriate mathematical model for the problem must now be (at least) spatially two-dimensional.

Let $[L(X, Y, T)], [S(X, Y, T)], [LS(X, Y, T)]$ and $[LR(X, Y, T)]$ denote the concentration of *Dpp*, *Sog*, *Dpp–Sog* complexes, and *Dpp*-receptor complexes, respectively. The first three concentrations diffuse with coefficients of diffusion D_L, D_S, and D_{LS}, respectively, and the concentration of immobile receptor is fixed at every location (X, Y), possibly nonuniformly distributed over the solution domain. Then the system of equations governing the morphogen dynamics as indicated in Figure 3 consists of the following four coupled differential equations, three of them being second-order nonlinear PDE of the reaction-diffusion type while the other being a first-order ordinary diffferential equation (ODE):

$$\frac{\partial [L]}{\partial T} = D_L \nabla^2_{XY}[L] - k_{on}[L]\{[R] - [LR]\} + k_{off}[LR] - j_{on}[L][S] + (j_{off} + \tau j_{\text{deg}})[LS] + V_L(Y) \tag{1}$$

$$\frac{\partial [LR]}{\partial T} = k_{on}[L]\{[R] - [LR]\} - (k_{off} + k_{\text{deg}})[LR] \tag{2}$$

$$\frac{\partial [LS]}{\partial T} = D_{LS} \nabla^2_{XY}[LS] + j_{on}[L][S] - (j_{off} + j_{\text{deg}})[LS] \tag{3}$$

$$\frac{\partial [S]}{\partial T} = D_S \nabla^2_{XY}[S] - j_{on}[L][S] + j_{off}[LS] + V_S(Y) \tag{4}$$

with

$$\begin{Bmatrix} V_L(Y) \\ V_S(Y) \end{Bmatrix} = \begin{Bmatrix} \bar{V}_L H(-Y) \\ \bar{V}_S H(Y) \end{Bmatrix}, \qquad \nabla^2_{XY}(\,) = \frac{\partial^2(\,)}{\partial X^2} + \frac{\partial^2(\,)}{\partial Y^2}, \tag{5}$$

where $H(z)$ is the Heaviside unit step function, equal to unity for positive z and zero for $z < 0$.

In the four differential equations above, the parameters k_{on}, k_{off}, and k_{deg} are the binding rate constant, dissociation rate constant, and degradation rate constant, respectively, for *Dpp*-receptor complexes while j_{on}, j_{off} and j_{deg} are the corresponding rate constants for *Sog–Dpp* complexes. The parameter τ in (1) assume a value in the interval [0, 1] giving the fraction of *Dpp* freed up by the degradation of the bound morphogen complex and returned to the free morphogen pool available for binding with receptors or Sog molecules. There is no return if $\tau = 0$ and complete return if $\tau = 1$. The quantity $[R(X, Y)]$ in (1) and (2) is the initial *tkv* receptor concentration at the location (X, Y) before the onset of *Dpp* synthesis and $[R(X, Y)] - [LR(X, Y)]$ being the unoccupied receptor concentration at (X, Y) still available for binding with *Dpp*. Three special receptor distributions of interest in the subsequent development are as follows:

(1) A spatially uniform distribution with $[R(X, Y)] = [\bar{R}_0]$.
(2) A distribution $[R(X, Y)] = [R_h(X)]$ uniform in Y but with two different segments of uniform receptor expression in X as given by

$$[R_h(X)] = \begin{cases} \bar{R}_0(1 + \Delta) & (X < X_h) \\ \bar{R}_0 & (X > X_h) \end{cases}, \qquad \Delta > 0, \tag{6}$$

for some positive constant Δ_h.
(3) A distribution $[R_2(X)]$ with three uniform segments of receptor expression in the X direction as given by

$$[R_h(X)] = \begin{cases} \bar{R}_0(1 + \Delta_\ell) & (X < X_\ell) \\ \bar{R}_0 & (X_\ell < X < X_g) \\ \bar{R}_0(1 + \Delta_g) & (X_g < X) \end{cases} \tag{7}$$

for some positive constants Δ_ℓ and Δ_g.

The system of four differential equations (1)–(4) above is sixth-order in the spatial variables. Given the symmetry with respect to the dorsal and ventral midline, we need only to consider the problem for the rectangular part $\Omega_{XY} = \{(0, X_{\max}) \times (-\frac{1}{4}Y_{\max}, \frac{1}{4}Y_{\max})\}$ of the actual domain. Along the

boundary $\partial\Omega_{XY}$ of Ω_{XY}, we have the following homogeneous Neumann conditions

$$(X, Y) \in \partial\Omega_{XY}: \qquad \frac{\partial[L]}{\partial n} = \frac{\partial[LS]}{\partial n} = \frac{\partial[S]}{\partial n} = 0 \tag{8}$$

for all $T > 0$ where $\partial[G]/\partial n$ is the normal derivative of $[G]$ and $\partial\Omega_{XY}$ is the boundary of Ω_{XY}. The no flux conditions along $Y = \pm\frac{1}{4}Y_{\max}$ follow immediately from the symmetry of the developmental activities with respect to the dorsal mid-line and ventral mid-line. The no flux conditions along $X = 0$ and $X = X_{\max}$ are more difficult to justify except that there can be no flux in any direction at the poles of the prolate spheroidal shape embryo. A more realistic treatment of the problem using (prolate) spheroidal coordinates will be the subject of a separate investigation.

Until morphogens being generated at $T = 0$, the biological system was in quiescence so that we have the homogeneous initial conditions

$$T = 0: \qquad [L] = [LR] = [LS] = [S] = 0, \tag{9}$$

for all (X, Y) in Ω_{XY}. The system (1)–(9) defines an IBVP for the four unknown concentrations $[L]$, $[LR]$, $[LS]$, and $[S]$.

2.3. Nondimensionalization

To reduce the number of parameters in the problem, we introduce the normalized quantities

$$t = \frac{D}{Y_{\max}^2}T, \qquad \{x, x_h, x_\ell, x_g, x_{\max}, y\} = \left\{\frac{X}{Y_{\max}}, \frac{X_h}{Y_{\max}}, \frac{X_\ell}{Y_{\max}}, \frac{X_g}{Y_{\max}}, \frac{X_{\max}}{Y_{\max}}, \frac{Y}{Y_{\max}}\right\}, \tag{10}$$

$$\{f_L, g_L, h_L, f_S, g_S, h_S\} = \frac{Y_{\max}^2}{D}\{k_{off}, k_{deg}, k_{on}\bar{R}_0, j_{off}, j_{deg}, j_{on}\bar{R}_0\}, \tag{11}$$

$$\{A, B, C, S, \rho, \rho_h\} = \frac{1}{\bar{R}_0}\{[L], [LR], [LS], [S], [R], [R_h]\}, \tag{12}$$

$$\{v_L, v_S, \bar{v}_L, \bar{v}_S\} = \frac{Y_{\max}^2}{D\bar{R}_0}\left\{V_L, V_S, \bar{V}_L, \bar{V}_S\right\}, \quad \{d_A, d_C, d_S\} = \left\{\frac{D_L}{D}, \frac{D_{LS}}{D}, \frac{D_S}{D}\right\} \tag{13}$$

where D is the maximum of D_L, D_{LS}, and D_S and $\bar{R}_0$ is a representative magnitude of $[R]$. With these normalized quantities, we rewrite the IBVP in the following dimensionless form

$$\frac{\partial A}{\partial t} = d_A\nabla^2 A - h_L A(\rho - B) + f_L B - h_S AS + (f_S + \tau g_S)C + v_L, \tag{14}$$

$$\frac{\partial B}{\partial t} = h_L A(\rho - B) - (f_L + g_L)B, \tag{15}$$

$$\frac{\partial C}{\partial t} = d_C \nabla^2 C + h_S AS - (f_S + g_s)C, \tag{16}$$

$$\frac{\partial S}{\partial t} = d_S \nabla^2 S - h_S AS + f_S C + v_S, \tag{17}$$

where now $\nabla^2( ) = ( )_{,xx} + ( )_{,yy}$ is the Laplacian in the dimensionless variables $(x,\ y)$ in the rectangle $\Omega = \{(0, x_{\max}) \times (-\frac{1}{4}, \frac{1}{4})\}$. After normalization, the special receptor distributions will be written as

$$[R] = \bar{R}_0 \rho(x, y), \tag{18}$$

with

$$(i) \quad \rho_o(x, y) = 1, \tag{19}$$

$$(ii) \quad \rho_h(x, y) = \begin{cases} \bar{\rho}_h \equiv 1 + \Delta > 1 & (x < x_h) \\ 1 & (x > x_h) \end{cases}, \tag{20}$$

$$(iii) \quad \rho_2(x, y) = \begin{cases} \bar{\rho}_1 \equiv 1 + \Delta_\ell & (x < x_\ell) \\ 1 & (x_\ell < x < x_g) \\ \bar{\rho}_2 \equiv 1 + \Delta_g & (x > x_g) \end{cases}. \tag{21}$$

For synthesis rates, we will be mainly concerned with the special case

$$\begin{Bmatrix} v_L(y) \\ v_S(y) \end{Bmatrix} = \begin{Bmatrix} \bar{v}_L H(-y) \\ \bar{v}_S H(y) \end{Bmatrix} \tag{22}$$

where $H(z)$ is the Heaviside step function.

The boundary conditions now take the form

$$(x, y) \in \partial\Omega: \quad \frac{\partial A}{\partial n} = \frac{\partial C}{\partial n} = \frac{\partial S}{\partial n} = 0 \tag{23}$$

for $t > 0$ where $\partial\Omega$ is the boundary of Ω. The homogeneous initial conditions become

$$t = 0: A = B = C = S = 0, \qquad (x, y) \epsilon\, \Omega. \tag{24}$$

2.4. Time-independent steady state

Similar to what was proved in [15], we expect the various initial concentrations of our embryo to evolve toward a time independent steady-state behavior. For

this steady-state solution, we have $\partial(\,)/\partial t = 0$ so that the governing PDE and boundary conditions become

$$\nabla^2 A - h_L A(\rho - B) + f_L B - h_S AS + (f_S + \tau g_S)C + \bar{v}_L H(-y) = 0, \quad (25)$$

$$h_L A(\rho - B) - (f_L + g_L)B = 0, \quad (26)$$

$$\nabla^2 C + h_S AS - (f_S + g_S)C = 0, \quad (27)$$

$$\nabla^2 S - h_S AS + f_S C + \bar{v}_S H(y) = 0, \quad (28)$$

where we have set $d_A = d_C = d_S = 1$ to simplify the discussion though the method of analysis employed is also applicable to the more general case. We can solve (26) for $B(x,y)$ in terms of $A(x,y)$ to get

$$B(x,y) = \frac{\rho(x,y)A(x,y)}{\alpha_L + A(x,y)}, \qquad \alpha_L = \frac{1}{h_L}(f_L + g_L), \quad (29)$$

and use the result in (29) to eliminate $B(x,y)$ from (25) to get

$$\nabla^2 A - \frac{\rho g_L A}{\alpha_L + A} - h_S AS + (f_S + \tau g_S)C + \bar{v}_L H(-y) = 0. \quad (30)$$

Equations (27), (28), and (30) form a sixth-order system of three second-order PDE for $A(x,y)$, $C(x,y)$, and $S(x,y)$. Augmented by the boundary conditions (23), this system can be solved by various numerical methods for elliptic boundary value problems. However, to gain insight to the qualitative behavior of the steady state, we also obtain instead an approximate solution in the context of the method of matched asymptotic expansions.

3. Matched asymptotic expansions for $\bar{V}_L/\bar{V}_S \ll 1$

3.1. Re-scaling of steady-state problem

It is rather typical in the development of *Drosophila* of interest here that the synthesis rate for *Sog* is substantially higher than that for *Dpp*. With $\varepsilon = \bar{v}_L/\bar{v}_S = \bar{V}_L/\bar{V}_S \ll 1$, the BVP for the steady-state behavior is amenable to an asymptotic solution by the method of matched asymptotic expansions. For this purpose, we re-scale the dimensionless steady state BVP by observing that both $S(x)$ and $C(x)$ are expected to be $O(\bar{v}_S)$. On the other hand, we expect $A(x)$ to be $O(\bar{v}_L)$ at most, in fact quite a bit smaller because available free *Dpp* should eventually be bound to *Sog* or receptors given that there is an abundance of *Sog* molecules. We, therefore, set

$$S = \bar{v}_S s(x, y, \varepsilon), \quad C = \frac{\bar{v}_S c(x, y, \varepsilon)}{f_S + g_S}, \quad A = \frac{\bar{v}_L}{\mu_L^2} a = \alpha_L \beta_L a(x, y, \varepsilon), \quad (31)$$

with

$$\varepsilon = \frac{\bar{v}_L}{\bar{v}_S} = \frac{\bar{V}_L}{\bar{V}_S}, \qquad v_L^* = \frac{h_S}{h_L}\frac{\bar{v}_L}{\sigma_L}, \qquad \beta_L = \frac{\bar{v}_L}{g_L}, \tag{32}$$

$$\sigma_L = \frac{g_L}{f_L + g_L}, \quad \mu_L^2 = \frac{g_L}{\alpha_L}, \quad \sigma_S = \frac{g_S}{f_S + g_S}, \quad \alpha_S = \frac{g_S + f_S}{h_S}, \tag{33}$$

and re-write (30), (27), and (28) as

$$\varepsilon\left\{\mu_L^{-2}\nabla^2 a - \frac{\rho a}{1+\beta_L a} + H(-y)\right\} - \left(v_L^* as - c\right) = 0, \tag{34}$$

$$(f_S + g_S)^{-1}\nabla^2 c + \left(v_L^* as - c\right) = 0, \tag{35}$$

$$\nabla^2 s - \left(v_L^* as - c\right) - \sigma_S c + H(y) = 0, \tag{36}$$

where we have taken $\tau = 1$ to simplify the presentation though the analysis would apply to other values of τ in (0, 1). The remaining unknown $B(x,y)$ is then given in terms of $a(x,y;\varepsilon)$ by (29) written as

$$B(x,y) = \frac{\rho(x,y)\beta_L a(x,y;\varepsilon)}{1+\beta_L a(x,y;\varepsilon)} \equiv b(x,y;\varepsilon). \tag{37}$$

For $\varepsilon = \bar{v}_L/\bar{v}_S \ll 1$, we seek an outer asymptotic expansion solution in parametric series of ε:

$$\{a(x,y;\varepsilon), b(x,y;\varepsilon), c(x,y;\varepsilon), s(x,y;\varepsilon)\} = \sum_{n=0}^{\infty}\{a_n(x,y), b_n(x,y), c_n(x,y), s_n(x,y)\}\varepsilon^n. \tag{38}$$

3.2. Leading term outer solution

The leading terms $a_0(x, y)$, $b_0(x, y)$, $c_0(x, y)$, and $s_0(x, y)$ correspond to the limiting case of $\varepsilon = 0$ (for $\bar{V}_S = \infty$). For this limiting case, Equations (34)–(36) reduce to

$$v_L^* a_0 s_0 - c_0 = 0, \qquad \nabla^2 c_0 = 0, \qquad \nabla^2 s_0 - \sigma_S c_0 + H(y) = 0 \tag{39}$$

and the boundary conditions (23) applied to the leading term quantities.

The second equation in (39) is for $c_0(x,y)$ alone. Together with the homogeneous Neumann condition along the edges of the rectangle, $\partial\Omega$, it requires

$$c_0(x, y) = \bar{c}_0. \tag{40}$$

To determine the constant $\bar{c}_0$, we integrate the last equation in (39) over the Ω and apply Green's theorem. The Neumann condition on s_0 along $\partial\Omega$ and the result (40) are then used to give

$$0 = \int\int_{\Omega} \left\{\nabla^2 s_0 - \sigma_S c_0 + H(y)\right\} dx\, dy$$
$$= -\sigma_S \bar{c}_0 x_{\max} + \frac{1}{2} x_{\max},$$

or

$$c(x, y) \sim c_0(x, y) = \bar{c}_0 = \frac{1}{2\sigma_S}. \tag{41}$$

The value for $\bar{c}_0$ in turn simplifies the last equation of (39) to

$$\nabla^2 s_0 = \frac{1}{2}\{H(-y) - H(y)\} \tag{42}$$

with s_0 required to satisfy the homogeneous Neumann condition along $\partial\Omega$. The solution of this BVP is

$$s_0(x, y) = s_0(y) = \begin{cases} \bar{s}_0 + \dfrac{1}{8}(y + 2y^2) & (y < 0) \\ \bar{s}_0 + \dfrac{1}{8}(y - 2y^2) & (y > 0) \end{cases} \tag{43}$$

where $\bar{s}_0$ is a constant of integration to be determined by the $O(\varepsilon)$ problem. Note that s_0 is (uniform in x and) continuously differentiable but has a simple jump discontinuity in $\partial^2 s_0/\partial y^2$ across $y = 0$.

Except for the unknown constant $\bar{s}_0$, we have also $a_0(x, y) = a_0(y)$ from the first equation in (44):

$$2\sigma_S v_L^* a_0(y; \bar{s}_0) = 2\sigma_S \frac{c_0}{s_0} = \begin{cases} \left[\bar{s}_0 + \dfrac{1}{8}(y + 2y^2)\right]^{-1} & (y < 0) \\ \left[\bar{s}_0 + \dfrac{1}{8}(y - 2y^2)\right]^{-1} & (y > 0) \end{cases}, \tag{44}$$

which also does not depend on x, and from (37) the leading term solution for $B(x,y)$

$$b_0(x, y) = \frac{\rho(x, y)\beta_L a_0(y; \bar{s}_0)}{1 + \beta_L a_0(y; \bar{s}_0)}, \tag{45}$$

which does depend on x (as well as y) through $\rho\ (x, y)$.

3.3. The O(ε) problem

To determine the unknown constant $\bar{s}_0$, we consider the $O(\varepsilon)$ problem for $a_1(x, y), \ldots, s_1(x, y)$. The governing equations for these unknowns are

$$(f_S + g_S)^{-1}\nabla^2 c_1 + \left[v_L^*(a_0 s_1 + a_1 s_0) - c_1\right] = 0, \tag{46}$$

$$\nabla^2 s_1 - \sigma_S c_1 - \left[v_L^*(a_0 s_1 + a_1 s_0) - c_1\right] = 0, \tag{47}$$

$$\mu_L^{-2}\nabla^2 a_0 - \frac{\rho a_0}{1+\beta_L a_0} + H(-y) - \left[v_L^*(a_0 s_1 + a_1 s_0) - c_1\right] = 0, \tag{48}$$

with

$$b_1(x, y) = \frac{\rho(x, y)\beta_L a_1}{(1+\beta_L a_0)^2}. \tag{49}$$

The unknowns a_1, c_1, and s_1 are subject to the homogeneous Neumann conditions (8) which also apply to the $O(\varepsilon)$ terms of the problem.

We begin to determine $\bar{s}_0$ by integrating (46) over Ω. Upon application of the two-dimensional divergence theorem and the homogeneous Neumann condition on s_1, we obtain

$$\int\int_\Omega \left[v_L^*(a_0 s_1 + a_1 s_0) - c_1\right] dx\, dy = 0. \tag{50}$$

This relation enables us to simplify the corresponding integral of (48) to

$$\int\int_\Omega \left\{\mu_L^{-2}\nabla^2 a_0 - \frac{\rho(x, y)a_0}{1+\beta_L a_0} + H(-y)\right\} dx\, dy = 0$$

or, upon application of the two-dimensional divergence theorem and the homogeneous Neumann condition on a_0,

$$J(\bar{s}_0) \equiv \int\int_\Omega \frac{\rho(x, y)a_0(y; \bar{s}_0)}{1+\beta_L a_0(y; \bar{s}_0)}\, dx\, dy = \frac{x_{\max}}{4}. \tag{51}$$

For any prescribed distribution of *tkv* concentration $\rho(x, y)$, this is a condition on $a_0(y; \bar{s}_0)$ alone and thus determining $\bar{s}_0$ in view of (44).

We may continue the solution process to solve (46)–(48) and the corresponding homogeneous Neumann conditions to determine c_1, s_1 and a_1. While this BVP is now truly two-dimensional given the explicit appearance of $\rho(x)$ in (48), the problem is actually tractable (by the method of eigenfunction expansions for example) because it is linear. However, we will not be concerned with the results for these higher order terms here but only note the following:

PROPOSITION 1. *For $\varepsilon = \bar{V}_L/\bar{V}_S \ll 1$, a formal leading outer (asymptotic expansion) solution for the re-scaled steady-state concentrations of (31) is given by (41), (43), and (44) with the parameter $\bar{s}_0$ in these expressions determined by (51). The corresponding concentration of the leading term signaling Dpp-receptor complex is given by (45).*

The results deduced from the leading term outer solution of the problem will obviously be modified by higher order terms in the outer asymptotic expansions (38) of the solution. However, the qualitative features of the outer

solution are not expected to be changed by such refinements for sufficiently small ε.

3.4. Inner solution and receptor saturation

Whenever an outer solution for $\varepsilon = \bar{V}_L/\bar{V}_S < 1$ is applicable, the leading term solution of Proposition 1 generally captures the qualitative effects of localized ectopic receptor expression with quantitative accuracy improves as ε decreases. However, the formal solution of Proposition 1 may not be applicable even if the condition $\varepsilon = \bar{V}_L/\bar{V}_S \ll 1$ is met. Of the two factors limiting its applicability, the possibility of supplementary inner asymptotic expansion solutions adjacent to the solution domain boundaries and discontinuities of system properties turn out not to be an issue for our problem. Given the homogeneous Neumann boundary conditions (8) along $\partial\Omega$, there should not be any sharp gradients (leading to layer solution components comparable to the outer solution in magnitude) adjacent to the edges of Ω. It is also evident from (30) that there can be at most a finite jump discontinuity in the *second derivatives* of $A(x,y)$ associated with jump discontinuities of the morphogen synthesis rates $V_L(X,Y)$ and $V_S(X,Y)$ and possible jump discontinuities of the receptor concentration $R(X, Y) = \bar{R}_0\rho(x, y)$. By (30), (28), and (27), the concentrations A, S, and C and their derivatives are expected to be continuous (with $[LS] = \bar{R}_0 C$ having even higher continuous derivatives) there. The only observable effect of the various discontinuous system properties is seen from the algebraic relation in (29) for $[LR] = \bar{R}_0 B$ (see also (37) and (45)) which is calculated from the solution for A after the implementation of the method of matched asymptotic expansions. These qualitative conclusions from the form of the PDE for the steady-state problem are supported by the results of numerical simulations of the original initial-boundary value problem on the evolution of the various concentrations starting from the onset of morphogen synthesis.

The other factor limiting the applicability of the outer asymptotic solution of the Proposition 1 comes from our choice of a model with fixed receptor concentration. For sufficiently large *Dpp* synthesis rates (but still small compared to the *Sog* synthesis rate), the *Dpp* synthesized may form such a high concentration of *Dpp*-receptor complexes to saturate the fixed receptor concentration. To the extent that our analytical method of solution of for the steady-state problem has no built-in mechanism for enforcing the constraint $[LR] \leq \bar{R}_0$, the formal asymptotic solution may be an erroneous description of the steady-state signaling gradient. As we see from an example in a later section, a formal asymptotic solution without enforcing the upper bound on $[LR]$ may result in an (outer) asymptotic solution with $[LR] > \bar{R}_0$ and/or morphogen concentrations such as $[L]$ and $[S]$ may become negative. As such, the matched asymptotic solution (whose leading term outer solution is summarized in Proposition 1) is not the appropriate steady-state solution for

our problem when $\bar{V}_L$ is high for the prescribed $\bar{R}_0$ even if the condition $\varepsilon = \bar{V}_L/\bar{V}_S < 1$ is met.

We note for emphasis that, for the low receptor saturation case, we do not need to consider explicitly the relevant inner solutions of the problems even in the neighborhood of the various synthesis rate and receptor expression discontinuities. For one reason, layer solution components, if any, do not affect the *Dpp, Sog*, and *Sog–Dpp complex* concentrations (and their first derivatives) in a qualitatively significant way throughout the solution domain. In addition, the Dpp-receptor concentration is computed after the process of matched asymptotic expansion solution for the BVP. Hence, we will focus our attention on some possible effects of morphogen synthesis rates and ectopic receptor expressions on the signaling morphogen concentration [*LR*] in the next few sections. These will be deduced from the outer solution when applicable and on numerical simulations of the IBVP otherwise.

3.5. Numerical simulations

It was pointed out in the previous two sections that for $\varepsilon = \bar{V}_L/\bar{V}_S \ll 1$, a leading term outer solution suffices for describing accurately the effect of ectopic receptor expression prior to receptor saturation. For a *Dpp* synthesis rate sufficiently high to result in receptor saturation, effects of ectopic receptor concentration are generally at variance with the matched asymptotic solution even for $\varepsilon \ll 1$ and may vary in rather complex ways depending on the values of the remaining system parameters. To uncover other possibilities regarding depressed or elevated [*LR*] concentration, we will establish in the next section some analytical properties of the outer asymptotic solution which should hold for the exact solution at low receptor saturation and low Dpp-to-Sog synthesis rate ratio. These results are complemented by numerical simulations of the original IBVP by a finite difference scheme (see [26]). In this finite difference approach, the diffusion terms are approximated by the second-order central difference and the adaptive Runge–Kutta–Fehlberg 2-3 method [27] is used for the temporal discretization. Convergence of the calculations and better resolution are observed when the spatial meshes are refined. The overall accuracy of numerical simulations is second-order in space and third-order in time.

The time evolution simulation code developed for the approach above has been validated by comparing results obtained for the special case of uniform receptor expression (with $\rho(x, y) = \rho_o(x, y) \equiv 1$) investigated in [15] with those shown in Figure 2 of that paper. The simulation code for the two-dimensional model of this paper when applied to the uniform receptor expression problem for the same set of parameter values as in [15] gives numerical results that are effectively identical to those obtained in Figure 2 of [15] with the corresponding values of [*LR*] at the dorsal midline agreeing to the three significant figures.

As an independent consistency check, the steady-state value of $[LR]$ from the simulation code was found to be essentially the same as that calculated from the steady-state value of $[L]$ using the steady-state relation (see (29))

$$[L\,R] = \frac{R(X, Y)[L]}{\bar{R}_0\alpha_L + [L]}. \tag{52}$$

The validated code for numerical solutions of the initial-boundary value problem for the reaction-diffusion system (14)–(17) will be used extensively to study the effects of ectopic receptor expression in the next few sections especially for the problem in [13] which stimulated this research. Typically, simulations were run until $T = 20$ hr and the prescribed stringent change tolerance had already been met. The non-monotone approach to steady state and the substantial changes between the initial state and the steady state of the $[LR]$ gradient for our class of *Dpp–Sog* interaction problems have been documented extensively in [13]. It is therefore prudent to evolve the various morphogen gradients for an unusually long period to ensure steady state. A direct solution for the steady-state problem is also possible and are being carried out separately. A time evolution simulation approach is preferred here to facilitate comparison with the one-dimensional results in [13].

4. Effects of ectopic receptor expression

4.1. The properties of $J(\bar{s}_0)$

To examine the effects of localized over-expression of *tkv* in the *Drosophila* embryo as determined by Proposition 1, we establish presently some properties of the function $J(\bar{s}_0)$ in (51) and their consequences, focusing on the receptor distributions $R(x, y) = \bar{R}_0$ (so that $\rho(x,y) = \rho_o(x,y) \equiv 1$) and $R(x,y) = R_h(x) \equiv \bar{R}_0\rho_h(x)$ (as given by (6)) in this section.

LEMMA 2. *$J(\bar{s}_0)$ is a monotone decreasing function of $\bar{s}_0$.*

Proof: For any fixed y, we have from the explicit solution for $a_0(y)$ in (44)

$$\frac{\partial a_0(y;\bar{s}_0)}{\partial \bar{s}_0} = \begin{cases} -\bar{c}_0\left[\bar{s}_0 + \dfrac{1}{8}(y + 2y^2)\right]^{-2} & (y < 0) \\ -\bar{c}_0\left[\bar{s}_0 + \dfrac{1}{8}(y - 2y^2)\right]^{-2} & (y > 0) \end{cases}$$

so that $\partial a_0(y;\bar{s}_0)/\partial\bar{s}_0 < 0$. Because $\rho(x)$ is positive, this implies

$$\frac{dJ(\bar{s}_0)}{d\bar{s}_0} = \int\int_\Omega \frac{\rho(x, y)}{[1 + \beta_L a_0(y;\bar{s}_0)]^2}\frac{\partial a_0(y;\bar{s}_0)}{\partial\bar{s}_0}\,dx\,dy < 0.$$

■

For (43) and (44) to be applicable, we must have $\bar{s}_0 > 0$ in order for $s_0(y;\bar{s}_0)$ and $a_0(y;\bar{s}_0)$ to be nonnegative. Hence $J(\bar{s}_0)$ is also positive. By Lemma 2, $J(\bar{s}_0)$ is a monotone decreasing function of $\bar{s}_0$; hence $J(\bar{s}_0)$ tends to 0 as $\bar{s}_0 \to \infty$. The argument proved the following result:

PROPOSITION 3. *$J(\bar{s}_0) = x_{\max}/4$ has exactly one positive root if $J(0) > x_{\max}/4$ and no positive solution if $J(0) < x_{\max}/4$.*

We now examine the root $\bar{s}_0 = \zeta$ of $J(\bar{s}_0) = x_{\max}/4$ for several distributions of the fixed receptor concentrations uniformly in the dorsal–ventral direction:

(a) Uniform Distribution $\rho(x,y) = \rho_o(x,y) \equiv 1$: For this case, the expression for $J(\bar{s}_0)$ involves only integration of a one-variable function:

$$J_o(\bar{s}_0) \equiv [J(\bar{s}_0)]_{\rho=\rho_o=1} = \int_0^{x_{\max}} \int_{-\frac{1}{4}}^{\frac{1}{4}} \left[\frac{a_0(y;\bar{s}_0)}{1+\beta_L a_0(y;\bar{s}_0)}\right] dx\, dy$$

$$\equiv \int_0^{x_{\max}} [I_o(\bar{s}_0)]\, dx = x_{\max}\, [I_o(\bar{s}_0)]\,, \tag{53}$$

where

$$I_o(z) = \int_{-\frac{1}{4}}^{\frac{1}{4}} \left[\frac{a_0(y;z)}{1+\beta_L a_0(y;z)}\right] dy. \tag{54}$$

Thus, with $\rho = \rho_o = 1$, the condition (51) determines $\bar{s}_0$ to be ς_0 with

$$\frac{1}{x_{\max}}\, [J_o(\bar{s}_0)]_{\bar{s}_0=\varsigma_0} = I_o(\varsigma_0) = \frac{1}{4}. \tag{55}$$

The expression (44) for $a_0(y;\bar{s}_0)$ can be used to re-write the integral in (54) as

$$J_o(\varsigma_0) = \frac{x_{\max}}{2\sigma_s v_L^*} \left[\int_{-\frac{1}{4}}^{0} \frac{dy}{\eta+\varsigma_0+\frac{1}{8}(y+2y^2)} + \int_0^{\frac{1}{4}} \frac{dy}{\eta+\varsigma_0+\frac{1}{8}(y-2y^2)}\right]$$

$$\equiv \frac{x_{\max}}{2\sigma_s v_L^*}[I_m(\varsigma_0) + I_p(\varsigma_0)] \equiv x_{\max}[I_o(\varsigma_0)], \tag{56}$$

and

$$\eta = \frac{\beta_L}{2\sigma_s v_L^*} = \frac{1}{2g_L}\frac{\sigma_L h_L}{\sigma_s h_S} = \frac{1}{2g_S}\frac{\alpha_S}{\alpha_L}. \tag{57}$$

The two integrals $I_m(\varsigma_0)$ and $I_p(\varsigma_0)$ in (56) can be evaluated exactly to give

$$\frac{16}{B_m(\varsigma_0)} \tan^{-1}\left(\frac{1}{B_m(\varsigma_0)}\right) + \frac{16}{B_p(\varsigma_0)} \tanh^{-1}\left(\frac{1}{B_p(\varsigma_0)}\right) = \frac{\sigma_s v_L^*}{2} \tag{58}$$

where

$$B_m(\xi) = 8\sqrt{\eta+\xi-\frac{1}{64}}, \qquad B_p(\xi) = 8\sqrt{\eta+\xi+\frac{1}{64}}. \tag{59}$$

Evidently, $I_o(z)$ is also a monotone decreasing function of z consistent with Lemma 2. More importantly, the following is an immediate consequent of (59).

LEMMA 4. *A positive* $\bar{s}_0$ *does not exist for* (51) *if* $\eta < 1/64$.

(b) Uniformly Elevated Anterior Receptor Distribution $\rho\ (x,y) = \rho_h(x)$: With $\rho_h(x)$ defined in (20), we have instead of (53)

$$J_h(\bar{s}_0) \equiv [J(\bar{s}_0)]_{\rho=\rho_h(x)} = \int_0^{x_{\max}} \int_{-\frac{1}{4}}^{\frac{1}{4}} \left[\frac{\rho_h(x) a_0(y;\bar{s}_0)}{1+\beta_L a_0(y;\bar{s}_0)} \right] dx\ dy$$

$$\equiv \int_0^{x_{\max}} [\rho_h(x) I_o(\bar{s}_0)]\, dx = (x_h \Delta + x_{\max})\, [I_o(\bar{s}_0)]\,. \tag{60}$$

The condition (51) determines $\bar{s}_0$ to be ς_h with

$$\frac{1}{x_{\max}} [J_o(\bar{s}_0)]_{\bar{s}_0=\varsigma_h} = (1+\delta_h \Delta) I_o(\varsigma_h) = \frac{1}{4}, \tag{61}$$

where $\delta_h = x_h/x_{\max} = X_h/X_{\max} < 1$, or

$$\frac{16}{B_m(\varsigma_h)} \tan^{-1}\left(\frac{1}{B_m(\varsigma_h)}\right) + \frac{16}{B_p(\varsigma_h)} \tanh^{-1}\left(\frac{1}{B_p(\varsigma_h)}\right) = \frac{\sigma_s v_L^*}{2(1+\delta_h \Delta)}. \tag{62}$$

(c) Relative Magnitude of ς_0 and ς_h: With (61) written as

$$I_o(\varsigma_h) = \frac{1}{4(1+\delta_h \Delta)} \tag{63}$$

where $I_o(z)$ is as defined in (54), we have then the following relative magnitude of the two roots ς_0 and ς_h:

PROPOSITION 5. $\varsigma_h \equiv [\bar{s}_0]_{\rho=\rho_h} > [\bar{s}_0]_{\rho=1} \equiv \varsigma_0$.

Proof: The claim follows immediately from $I_o(\varsigma_0) = \frac{1}{4} > 1/4(1+\delta_h \Delta) = I_o(\varsigma_h)$ and Lemma 2 for any positive X_h so that $\delta_h = x_h/x_{\max} = X_h/X_{\max} > 0$. ■

(d) Receptor Distribution Uniform in the Dorsal–Ventral Direction: For a piecewise continuous function of x alone, $\rho(x,y) = \rho_{vd}(x)$, we have

$$[J(\bar{s}_0)]_{\rho=\rho_{vd}(x)} \equiv J_{vd}(\bar{s}_0) = \int_0^{x_{\max}} \int_{-\frac{1}{4}}^{\frac{1}{4}} \left[\frac{\rho_{vd}(x) a_0(y;\bar{s}_0)}{1+\beta_L a_0(y;\bar{s}_0)} \right] dx\ dy$$

$$= \bar{\rho}_{vd} x_{\max} \int_{-\frac{1}{4}}^{\frac{1}{4}} \left[\frac{a_0(y;\bar{s}_0)}{1+\beta_L a_0(y;\bar{s}_0)} \right] dy. \tag{64}$$

With $a_0(y;\bar{s}_0)$ given by (44), the integral remaining in (64) can again be evaluated exactly with

$$J_{vd}(\bar{s}_0) = \frac{\bar{\rho}_{vd}x_{\max}}{2\sigma_s v_L^*}\left[\int_{-\frac{1}{4}}^{0}\frac{dy}{\tilde{s}_0+\frac{1}{8}(y+2y^2)}+\int_{0}^{\frac{1}{4}}\frac{dy}{\tilde{s}_0+\frac{1}{8}(y-2y^2)}\right]$$
$$\equiv \frac{\bar{\rho}_{vd}x_{\max}}{2\sigma_s v_L^*}[I_m(\bar{s}_0)+I_p(\bar{s}_0)] = x_{\max}\bar{\rho}_{vd}I_o(\bar{s}_0) \tag{65}$$

where

$$\bar{\rho}_{vd}x_{\max} = \int_0^{x_{\max}}\rho_{vd}(x)\,dx. \qquad \tilde{s}_0 = \bar{s}_0 + \frac{\beta_L}{2\sigma_S v_L^*} \equiv \bar{s}_0 + \eta. \tag{66}$$

A particular application of this type of ectopic receptor distributions will be discussed in Section 5.

It is also possible to investigate the effects of ectopic receptor distributions whose ectopicity varies in both the X and Y directions. We illustrate with the following example:

(e) Receptors Concentration Nonuniform in Both X and Y: The effect of a localized over-expression of *tkv* more akin to the one shown in panels A and B of Figure 1 for the *Drosophila* embryo is also possible. The distribution in panel A may be approximated by

$$[R_A(X,Y)] = \begin{cases}\bar{R}_0\{(1+\Delta)H(-y)+\Delta_\ell H(y)\} & (X<X_h)\\ \bar{R}_0\{1+\Delta_g\} & (X>X_h)\end{cases}, \tag{67}$$

or

$$\rho_A(x,y) = \frac{1}{\bar{R}_0}[R_A(X,Y)] = \begin{cases}(1+\Delta)H(-y)+\Delta_\ell H(y) & (x<x_h)\\ 1+\Delta_g & (x>x_h)\end{cases}, \tag{68}$$

where $\Delta > 0$, $\Delta_g \geq 0$ and $0 \leq \Delta_\ell \leq 1+\Delta$. For this dorsal–ventral nonuniform receptor distribution, Lemma 2 and Proposition 3 continue to hold because their proofs apply to all positive receptor concentration. Hence $J(\bar{s}_0)$ as defined in (51) continues to be a monotone decreasing function of $\bar{s}_0$ and $J(\bar{s}_0) = x_{\max}/4$ has exactly one root in $(0,\infty)$ if $J(0) > x_{\max}/4$.

4.2. Signaling receptor concentration

From (37), we have

$$\frac{[LR]}{\bar{R}_0} = B(x,y) = b(x,y;\varepsilon) = \frac{\rho(x,y)\beta_L a(x,y)}{1+\beta_L a(x,y)}$$
$$\sim \frac{\rho(x,y)\beta_L a_0(y;\bar{s}_0)}{1+\beta_L a_0(y;\bar{s}_0)} = \frac{\eta\rho(x,y)}{\eta+s_0(y;\bar{s}_0)} \tag{69}$$

where $s_0(y;\bar{s}_0)$ and η are given by (43) and (57), respectively.

(a) $\rho\ (x,\ y) = 1$: We have for this case $\bar{s}_0 = \varsigma_0$ and therewith

$$\frac{1}{\eta \bar{R}_0}[LR]_{\rho(x)=1} = \frac{1}{\eta}[b(x,\ y;\varepsilon)]_{\rho(x)=1} \sim \left[\frac{1}{\eta + s_0(y;\bar{s}_0)}\right]_{\bar{s}_0=\varsigma_0}$$
$$= \begin{cases} \left[\eta + \varsigma_0 + \frac{1}{8}(y + 2y^2)\right]^{-1} & (y < 0) \\ \left[\eta + \varsigma_0 + \frac{1}{8}(y - 2y^2)\right]^{-1} & (y > 0) \end{cases}. \tag{70}$$

(b) $\rho\ (x,\ y) = \rho_h(x)$: For this case, we have similarly $\bar{s}_0 = \varsigma_h$ and therewith

$$\frac{1}{\eta \bar{R}_0}[LR]_{\rho(x)=\rho_h(x)} = \frac{1}{\eta}\,[b(x,\ y;\varepsilon)]_{\rho(x)=\rho_h(x)} \sim \left[\frac{\rho_h(x)}{\eta + s_0(y;\bar{s}_0)}\right]_{\bar{s}_0=\varsigma_h}. \tag{71}$$

As a principal aim of our research effort, we wish to learn whether $[LR]$ is depressed outside the region of elevated receptor expression. For this posterior end range $x_h < x \leq x_{\max}$ where the normalized receptor concentration is unit, i.e., $\rho_h(x) = 1$, we have

$$\frac{1}{\eta \bar{R}_0}[LR]_{\rho_h(x)} \sim \left[\frac{1}{\eta + s_0(y;\bar{s}_0)}\right]_{\bar{s}_0=\varsigma_h}$$
$$= \begin{cases} \left[\eta + \varsigma_h + \frac{1}{8}(y + 2y^2)\right]^{-1} & (y < 0) \\ \left[\eta + \varsigma_h + \frac{1}{8}(y - 2y^2)\right]^{-1} & (y > 0) \end{cases}. \tag{72}$$

From this follows the next result which addresses the question that motivated this investigation:

PROPOSITION 6. *At low receptor occupation and the outer solution applicable, over-expressing Dpp receptors tkv on the anterior half of the embryo reduces PMad activation in cells on the posterior part of the embryo.*

Proof: The observation is an immediate consequence of (70), (71), and Proposition 5. ■

When the asymptotic solution of Section 3 applies, we now see that an elevated receptor concentration in the anterior end of the embryo invariably leads to a depression of signaling bound morphogen concentration posterior to the region of elevated receptor concentration, whether the depression is noticeable depends on the magnitude of the *Dpp* synthesis rate (with values of all other parameters fixed).

As for the effect of ectopic *tkv* expression on the signaling $[LR]$ at the anterior end of the embryo (the site of ectopic receptors), we have for $0 < x < x_h$

$$\frac{1}{\eta \bar{R}_0}[LR]_{\rho_h(x)} \sim \left[\frac{1+\Delta}{\eta + s_0(y;\bar{s}_0)}\right]_{\bar{s}_0=\varsigma_h} = \begin{cases} (1+\Delta)/\left[\eta + \varsigma_h + \frac{1}{8}(y+2y^2)\right] & (y<0) \\ (1+\Delta)/\left[\eta + \varsigma_h + \frac{1}{8}(y-2y^2)\right] & (y>0) \end{cases}. \tag{73}$$

The comparison with the corresponding expression for $\rho(x) = 1$ in the same region now depends on the magnitude of Δ, whether it is sufficiently large to compensate for the reduction by a larger $\bar{s}_0$ in the denominator. In particular, we have

PROPOSITION 7. *When the outer asymptotic solution applies, over-expressing Dpp receptors tkv on the anterior end of the embryo by a sufficiently large concentration so that*

$$1 + \Delta > \frac{\eta + \varsigma_h - \frac{1}{64}}{\eta + \varsigma_0 - \frac{1}{64}} \tag{74}$$

elevates PMad activation in cells on the part of the embryo with the ectopic receptors. The opposite is true if the inequality in (74) is reversed at least for a part contiguous to the dorsal midline.

4.3. Elevated anterior receptor expression

For the asymptotic solution to be applicable, it is necessary to have $\varepsilon = \bar{V}_L/\bar{V}_S \ll 1$, i.e., $\bar{V}_L$ must be small compared to $\bar{V}_S$. To illustrate the diverse range of possible steady-state configurations in different range of ε (within and outside the range $\varepsilon \ll 1$), the two-dimensional numerical simulation code is applied in this section to the problem investigated in Figure 5 of [13] which stimulated this research. In addition to $\bar{V}_L = 1\,\text{nM/s} = 10^{-3}\,\mu\text{M/s}$ and $\bar{V}_S = 0.08\,\mu\text{M/s}$ investigated in that figure, we also examine cases with $\bar{V}_L = 2.5 \times 10^{-4}\,\mu\text{M/s}$ and with $\bar{V}_S = 0.6\,\mu\text{M/s}$ and $10^{-3}\,\mu\text{M/s}$. The remaining values of the different parameters for the problem used in [13] are given in Table 1.

Remark 8. For these parameter values, we have $\alpha_L = (g_L + f_L)/h_L \simeq 4.37 \times 10^{-4}$, $\mu_L^2 = g_L/\alpha_L \simeq h_L = 4.27 \times 10^3$, and $\eta = 1.17 \times 10^{-3}$. We are

Table 1
Parameter Values

$D = D_L = D_S = D_{LS}$	$X_{\max}$	$Y_{\max}$	$\bar{R}_0$
8.5×10^{-7} cm^2 s^{-1}	5.5×10^{-2} cm	5.5×10^{-2} cm	$3.0\,\mu$M

$k_{on} \times 10$	$j_{on} \times 10^{-1}$	$k_{\deg} \times 10^4$	$j_{\deg} \times 10$	$k_{off} \times 10^6$	$j_{off} \times 10^6$
$4.0\,\mu\text{M}^{-1}\text{s}^{-1}$	$9.5\,\mu\text{M}^{-1}\,\text{s}^{-1}$	$5.0\,\text{s}^{-1}$	$5.4\,\text{s}^{-1}$	$4.0\,\text{s}^{-1}$	$4.0\,\text{s}^{-1}$

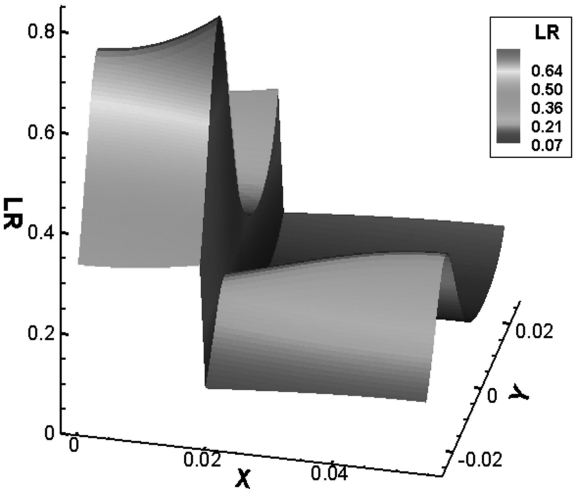

Figure 4. Two-dimensional plot of the [LR] distribution for the fixed receptor expression $R_h(X)$ (with ectopic expression in $0 \le X < X_h = 0.02$ cm) for $\bar{V}_L = 2.5 \times 10^{-4}$ μM/s and $\bar{V}_S = 0.6$ μM/s.

interested in cases corresponding to the six different combinations of values of $\bar{V}_L$ and $\bar{V}_S$ fixing other parameter values as given in Table 1.

With *Dpp* synthesized only in the dorsal region and diffused away from its localized source, the steady-state distribution of *Dpp* expression [L] is expected to reach its maximum at the dorsal midline $Y = -Y_{\max}/4$ and decreases monotonically in both directions toward its minimum at $Y = Y_{\max}/4$. Because the steady state [LR] is an increasing function of [L] (see (29) or (69)), it also attains its maximum at the dorsal midline $Y = -Y_{\max}/4$. Shown in Figure 4 is a two-dimensional plot of the steady-state signaling gradient [LR] for the case $R(X,Y) = R_h(X)$ with $\bar{V}_L = 0.25 \times 10^{-3}\,\mu$M/s and $\bar{V}_L = 0.6\,\mu$M/s. It provides the numerical evidence confirming these qualitative features of the [LR] expression. As such, we may focus our discussion on the signaling gradient along the dorsal midline assisted at times by one-dimensional plots of

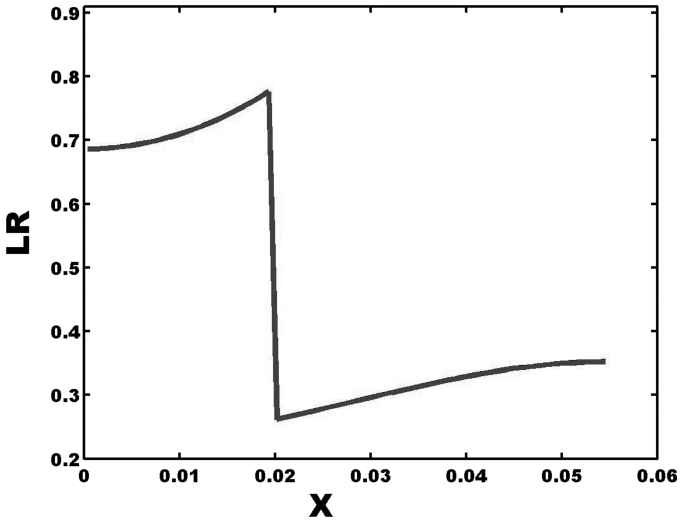

Figure 5. Distribution of $[LR]$ in the anterior–posterior direction at the dorsal midline for the fixed receptor expression $R_h(X)$ (with ectopic expression in $0 \leq X < X_h = 0.02\,\text{cm}$) for $\bar{V}_L = 2.5 \times 10^{-4}\ \mu\text{M/s}$ and $\bar{V}_S = 0.6\,\mu\text{M/s}$.

Table 2
Numerical Solution for $[LR]$ in μM at Dorsal Midline

$(\bar{V}_L = 0.25 \times 10^{-3}\,\mu\text{M/s})$					
$\bar{V}_S$	δ_h	$[LR]_{x=0}$	$[LR]_{x=x_h-}$	$[LR]_{x_h+}$	$[LR]_{x=x_{\max}}$
$10^{-3}\,\mu\text{M/s}$	0	0.5406..	0.5406..	0.5406..	0.5406..
	4/11	0.5126..	0.7452..	0.3530..	0.5426..
$8\times10^{-2}\,\mu\text{M/s}$	0	0.6314..	0.6314..	0.6314..	0.6314..
	4/11	0.5281..	0.7431..	0.2578..	0.6067..
$6\times10^{-1}\,\mu\text{M/s}$	0	0.6241..	0.6241..	0.6241..	0.6241..
	4/11	0.6859..	0.7762..	0.2618..	0.3522..
$\infty\,\mu\text{M/s}$	0	0.6239..	0.6239..	0.6239..	0.6239..
	4/11	0.7816..	0.7816..	0.2605..	0.2605..

midline graphs such as the one in Figure 5 for $[LR]$ at $Y = -Y_{\max}/4$. Given the level of $[LR]$ for a uniform receptor expression reported in Table 2 (in rows with $\delta_h = 0$), it is clear that the signaling gradient is now depressed at the posterior end (where there is the same uniform receptor expression) and elevated at the anterior end (where there is an ectopic receptor expression), at least in an interval adjacent to X_h. The elevation and depression become

more uniform in $X < X_h$ and $X > X_h$, respectively, for higher Sog synthesis rates V_S.

Starting from quiescence, the non-monotone approach to the steady behavior of the *Dpp–Sog* interaction has been found to be similar to the one-dimensional problem already discussed extensively in [13]. Hence, it will not be further elaborated herein. Instead, we will present results on the steady-state [*LR*] at different locations of the dorsal midline in the direction of the anero–posterior axis to illustrate the complexity of possible outcomes of the same ectopic receptor expression depending on the magnitude of the two ligand synthesis rates (with all other wing disc rate constants fixed). We will discuss separately the signaling gradient for two particular values of the *Dpp* synthesis rate, first for $\bar{V}_L = 0.25 \times 10^{-3}\,\mu$M/s and then for $\bar{V}_L = 10^{-3}\,\mu$M/s for which some observations were given in [13].

4.3.1. *Signaling morphogen gradient [LR] for* $\bar{V}_L = 0.25 \times 10^{-3}\,\mu$M/s. In Table 2, the signaling morphogen gradient [*LR*] at the dorsal midline are given for $\bar{V}_L = 0.25 \times 10^{-3}\,\mu$M/s. The results for a uniform receptor expression (with $\bar{R}_0 = 3\,\mu$M) throughout the solution domain are given in the odd rows (with $\delta_h = 0$) for $\bar{V}_S = \{0.001, 0.08, 0.6 \text{ and } \infty\}\,\mu$M/s, respectively. The results for $\bar{V}_S = \infty$ corresponds to those obtained from the outer asymptotic solution while those for finite $\bar{V}_S$ were obtained by the simulation code for the IBVP. For a uniform receptor distribution, the dorsal midline values of [*LR*] shown are independent of X as expected and tend to the asymptotic solution as $\bar{V}_S$ increases from 0.08 to $0.6\,\mu$M/s with the latter nearly equal to the asymptotic value. For $\bar{V}_S = 1$ nM/s $= 10^{-3}\,\mu$M/s however, we have $\varepsilon = \frac{1}{4}$ so that the *Sog* synthesis rate is relatively low leading to a level of *Sog* concentration in steady state that is too low to shuttle enough *Dpp* back to the anterior end for additional binding with available receptors to achieve the level of [*LR*] given by the outer asymtptotic solution.

The even rows in Table 2 with $\delta_h = 4/11$ give the corresponding results for a localized elevated receptor expression $R_h(X)$ (see (6)). In the interval $X_h < X \le X_{\max}$, a comparison of the steady state [*LR*] concentration for the two different receptor expressions clearly shows a close agreement between the asymptotic and simulation values of [*LR*] at the dorsal midline near the X_h and less so near the end $X_{\max}$. The agreement throughout the interval gets better as $\bar{V}_S$ increases from $0.08\,\mu$M/s and more *Dpp* molecules are shuttled away by a higher concentration of *Sog*. There is clearly a depression of [*LR*] concentration in the posterior portion of the solution domain $X > X_h$ (as well as a qualitative agreement even for the case $\bar{V}_S = 1$ nM/s ($\varepsilon = 1$) for which the asymptotic solution is not applicable.)

In the region with elevated receptor expression, $0 \le X < X_h$, the situation is more complicated. The outer asymptotic steady-state solution for the receptor distribution $R_h(X)$ shows a higher steady-state [*LR*] concentration than the

corresponding (uniform) concentration for a uniform receptor distribution throughout the sub-interval $[0, X_h)$. On the other hand, the numerical solutions for the IBVP shows a higher $[LR]$ concentration only for $\bar{V}_S = 0.6\,\mu$M/s; moreover, the elevation in $[LR]$ for this (and other) *Sog* synthesis rate is nonuniform, closer to the asymptotic solution near X_h and considerably smaller near $X = 0$. Because the asymptotic steady-state solution for $[LR]$ does not depend on $\bar{V}_S$ (or more correctly corresponds to the limiting case of $\bar{V}_S = \infty$), the lower level of $[LR]$ near $X = 0$ appears to be due to less *Dpp–Sog* binding and hence more *Dpp*-receptor binding resulting in more receptor-mediated degradation of *Dpp* for the given moderate synthesis rate $\bar{V}_L$.

For $\bar{V}_S = 0.08\,\mu$M/s, numerical solutions show an elevated level of $[LR]$ only for the part of the interval $[0, X_h)$ near $X = X_h$, the location for the abrupt change of receptor expression. For this lower *Sog* synthesis rate (which is still large compared to the *Dpp* synthesis rate), $[LR]$ is actually depressed near the end $X = 0$. The nonuniform distribution in the antero-posterior direction reflects the fact that receptors near X_h has the rights of first refusal to bind with *Dpp* freed up from the degradation of the *Dpp-Sog* complexes being transported back to the anterior end. For the given $\bar{V}_L$ and a lower $\bar{V}_S$ such as $0.08\,\mu M/s$, the amount of *Sog* produced does not lead to a sufficiently large concentration of *Dpp–Sog* to be transported to the anterior end and degrade, freeing up sufficient *Dpp* to diffuse further away from X_h for the unoccupied receptors near $X = 0$.

To put it another way, for a fixed *Dpp* synthesis rate, we get an elevated expression of $[LR]$ at the tip of the anterior compartment away from the location of the abrupt change in receptor expression at X_h of $R_h(X)$ only if the *Sog* synthesis rate is sufficiently high. When all other biological rate constants of the embryo are held fixed, we need a high level of *Sog* expression for the formation of a level of $[LS]$ concentration to be transported from the ventral region back to the entire dorsal region, to dissociate and degrade, freeing up enough *Dpp* to be binding with receptor *tkv* everywhere in the anterior compartment. At the same time, it appears from numerical solutions of the IBVP that the abrupt change of receptor expression at X_h would invariably results in a boundary layer phenomenon on both sides of the discontinuity of the receptor distribution. The elevation and depression of the steady-state signaling $[LR]$ concentration in a narrow region (in the anterior and posterior side, respectively) adjacent to X_h are more pronounced than expected from the informal asymptotic consideration.

4.3.2. *Non-signaling gradients for* $\bar{V}_L = 0.25 \times 10^{-3}\,\mu$M/s. When the asymptotic steady-state solution is applicable, there is also a close agreement between the asymptotic and simulation results for $[LS]$, $[S]$, and $[L]$ except for the expected spatial nonuniformity in both X and Y directions with the latter similar to those shown in Figure 5 in [15]. The corresponding

Table 3
Asymptotic and Numerical Results in μM at Dorsal Midline

	($\bar{V}_L = 0.25 \times 10^{-3}\,\mu$M/s, $\bar{V}_S = 0.08\,\mu$M/s)					
	$\bar{V}_S$	δ_h	$x = 0$	$x = x_h-$	$x = x_h+$	$x = x_{\max}$
	∞	0	$0.74.. \times 10^{-1}$	$0.74.. \times 10^{-1}$	$0.74.. \times 10^{-1}$	$0.74.. \times 10^{-1}$
	∞	4/11	$0.74.. \times 10^{-1}$	$0.74.. \times 10^{-1}$	$0.74.. \times 10^{-1}$	$0.74.. \times 10^{-1}$
$\frac{[LS]}{\mu\text{M/s}}$	–	–	–	–	–	–
	0.08	0	$0.75.. \times 10^{-1}$	$0.75.. \times 10^{-1}$	$0.75.. \times 10^{-1}$	$0.75.. \times 10^{-1}$
	0.08	4/11	$0.70.. \times 10^{-1}$	$0.75.. \times 10^{-1}$	$0.75.. \times 10^{-1}$	$0.86.. \times 10^{-1}$
		*		*		*
	∞	0	$0.33.. \times 10^{-3}$	$0.33.. \times 10^{-3}$	$0.33.. \times 10^{-3}$	$0.33.. \times 10^{-3}$
	∞	4/11	$0.12.. \times 10^{-3}$	$0.12.. \times 10^{-3}$	$0.12.. \times 10^{-3}$	$0.12.. \times 10^{-3}$
$\frac{[L]}{\mu\text{M/s}}$	–	–	–	–	–	–
	0.08	0	$0.34.. \times 10^{-3}$	$0.34.. \times 10^{-3}$	$0.34.. \times 10^{-3}$	$0.34.. \times 10^{-3}$
	0.08	4/11	$0.12.. \times 10^{-3}$	$0.17.. \times 10^{-3}$	$0.17.. \times 10^{-3}$	$0.40.. \times 10^{-3}$
		*		*		*
	∞	0	$0.12.. \times 10^{1}$	$0.12.. \times 10^{1}$	$0.12.. \times 10^{1}$	$0.12.. \times 10^{1}$
	∞	4/11	$0.35.. \times 10^{1}$	$0.35.. \times 10^{1}$	$0.35.. \times 10^{1}$	$0.35.. \times 10^{1}$
$\frac{[S]}{\mu\text{M/s}}$	–	–	–	–	–	–
	0.08	0	$0.13.. \times 10^{1}$	$0.13.. \times 10^{1}$	$0.13.. \times 10^{1}$	$0.13.. \times 10^{1}$
	0.08	4/11	$0.49.. \times 10^{1}$	$0.35.. \times 10^{1}$	$0.35.. \times 10^{1}$	$0.15.. \times 10^{1}$

asymptotic and numerical solutions for $[L]$, $[S]$, and $[LS]$ are given in Table 3 for $\bar{V}_S = 0.08\,\mu$M/s to demonstrate the qualitative agreement for this set of parameter values, particularly near $X = X_h$. The nonuniformity in the X direction is more pronounced for $[L]$ and $[S]$. The variation with X (computed but not shown here) reduces considerably for $\bar{V}_S = 0.6\,\mu$M/s or larger.

4.3.3. *Signaling morphogen gradient [LR] for* $\bar{V}_L = 10^{-3}\,\mu$M/s. For a sufficiently high *Dpp* synthesis rate, there would be more than enough *Dpp* for binding to saturate the available *tkv* receptors (which is fixed in our model), at least in an interval $0 < |Y - Y_{\max}/4| < d_y$ centered at the dorsal midline along the posterior end of the embryo in steady state. This is evident from the dorsal midline values of $[LR]$ for the case of a uniform receptor expression shown in Table 4 for $\bar{V}_S = 0.6\,\mu$M/s and $0.08\,\mu$M/s. A graph of $[LR]$ at the dorsal midline for $\bar{V}_S = 0.6\,\mu$M/s is shown in Figure 6 to illustrate the saturation. Thus the higher *Dpp* synthesis rate $\bar{V}_L = 10^{-3}\,\mu$M/s coupled with a

Table 4
$[LR]$ at Dorsal Midline in μM ($\bar{V}_L = 10^{-3}\,\mu M/s$)

$\bar{V}_S$	δ_h	$[LR]_{x=0}$	$[LR]_{x=x_h-}$	$[LR]_{x_h+}$	$[LR]_{x=x_{\max}}$
$10^{-3}\,\mu$M/s	0	2.0432..	2.0432..	2.0432..	2.0432..
	4/11	1.9868..	2.9233..	1.4645..	1.9893..
$8\times10^{-2}\,\mu$M/s	0	2.9428..	2.9428..	2.9428..	2.9428..
	4/11	2.8211..	5.9636..	2.2612..	2.9456..
$6\times10^{-1}\,\mu$M/s	0	2.9934..	2.9934..	2.9934..	2.9934..
	4/11	4.1176..	8.0755..	2.8289..	2.9927..
$\infty\,\mu$M/s	0	7.8208..	7.8208..	7.8208..	7.8208..
	4/11	8.3495..	8.3495..	2.7832..	2.7832..

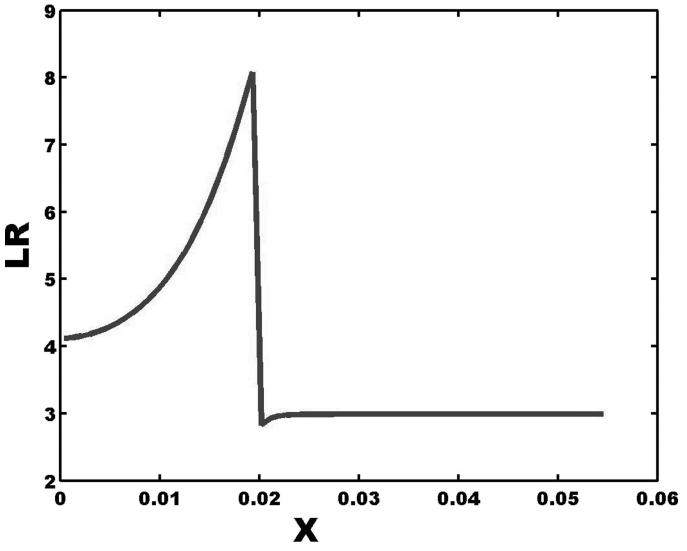

Figure 6. Distribution of $[LR]$ in the anterior–posterior direction at the dorsal midline for the fixed receptor expression $R_h(X)$ (with ectopic expression in $0 \le X < X_h = 0.02\,\text{cm}$) for $\bar{V}_L = 10^{-3}\,\mu$M/s and $\bar{V}_S = 0.6\,\mu$M/s.

sufficiently high *Sog* synthesis rate leads to a saturation of available receptors in the posterior segment. The asymptotic steady-state solution is not applicable in this case as the method of solution does not take into account receptor saturation. In fact, that solution gives a steady state $[LR]$ concentration in excess of the prescribed receptor concentration (see the case $\bar{V}_S = \infty$ in Table 4). The inappropriateness of such a solution is also reflected in its (unacceptable) negative steady-state concentrations for the free *Sog* and *Dpp* molecules (not shown herein).

At the lower *Sog* synthesis rate of $\bar{V}_S = 10^{-3}\,\mu$M/s, the steady-state $[LR]$ at the dorsal midline given in Table 4 is at about 1.98.. μM at the two ends of the embryo, which is nowhere near saturation for the available receptors (with $\bar{R}_0 = 3\,\mu$M) and seemingly consistent with that predicted by the outer asymptotic solution ($\simeq$ 2.04..). However, the agreement is somewhat fortuitous because the outer asymptotic solution also does not apply in this case given $\bar{V}_S = \bar{V}_L$ so that ε is not small compared to unity and a leading term regular perturbation solution is also mathematically inappropriate. Biologically, the expression of *Sog* at the ventral region is not sufficiently high so that not enough *Dpp* is transported to the dorsal region for binding with the available receptors in that region (except in the neighborhood of X_h where it is accomplished at the expense of similar activities near X_h on the posterior side).

While the results for $\bar{V}_L = 10^{-3}\,\mu$M/s in Table 4 clearly demonstrate the limitation of the outer asymptotic steady-state solution obtained in Section 3, they do not in any way diminish the value of the analytic solution because its applicability can easily be decided by examining whether the concentration of signaling Dpp-receptor complexes meets the restriction $[LR] \leq \bar{R}_0$ and whether the remaining concentration gradients are nonnegative (in addition to $\varepsilon \ll 1$). We simply do not use the outer asymptotic solution if any of the constraints is not met.

4.3.4. *Summary.* The developments in this section show the complementary nature of the analytical and numerical methods. The former has the advantage of exhibiting more explicitly the dependence of the solution on the various system parameters while the latter applies to a broader region in the parameter space. To simplify our analysis and computation, we have chosen to work with a model with a prescribed *tkv* receptor concentration fixed for all time. The restriction limits the applicability of the asymptotic solution developed in Section 3, which by nature does not take into account the constraint of a fixed receptor concentration during the solution process.

With all other rate parameters fixed, the asymptotic steady-state solution provides an adequate description of the signaling morphogen gradient concentration $[LR]$ for moderate *Dpp* synthesis rates $\bar{V}_L$ that do not saturate the fixed receptor concentration $\bar{R}_0$ (such as the case $\bar{V}_L = 2.5 \times 10^{-4}\,\mu$M/s reported in Table 2). For these moderate *Dpp* synthesis rates, the distribution of $[LR]$ in the anterior–posterior direction obtained by the (more accurate) numerical simulations tends to the asymptotic solution (with a uniform distribution on both sides of the receptor concentration discontinuity) for higher and higher *Sog* synthesis rates, e.g., for $\bar{V}_S = 0.6\,\mu$M/s or higher. More importantly (pertaining to the purpose of our investigation), these results established the existence of a depressed $[LR]$ concentration in the posterior end of the embryo when there is an ectopic receptor expression in the anterior

end. The asymptotic solution helps delineate more explicitly the mechanism responsible for the depression.

On the other hand, for relatively low *Sog* synthesis rates such as $\bar{V}_S = 0.08\,\mu$M/s, the $[LR]$ concentration near the anterior end $X = 0$ may even be, somewhat surprisingly, lower than the level for the case of a uniform receptor distribution, the elevated level of receptor concentration notwithstanding. An explanation for this somewhat unexpected result was given in Section 4.3.1.

For the same rate parameter values but higher *Dpp* synthesis rates at the level of $\bar{V}_L = 10^{-3}\,\mu$M/s, the available free *Dpp* eventually saturate the available receptors (of fixed concentration) for the *uniform* fixed receptor case and at least in the posterior region for the receptor distribution $R_h(x)$ ectopically expressed at the anterior end. For these cases, the asymptotic solution gives a signaling gradient $[LR]$ in excess of the available receptors in some region of the embryo (and possibly negative concentration for the *Sog* and *Dpp–Sog* gradients) and hence would be inappropriate for the problem. Such a limitation on the asymptotic steady-state solution would not be present in a model allowing for receptor renewal.

5. Signaling morphogen concentration for ectopic expression at both ends

5.1. Properties of $J(\bar{s}_0)$

If we examine panel *B* of Figure 1 more closely, we would see that there seems to be an over-expression of receptors at both ends of the anterior–posterior axis. To find out what our model would predict for this configuration of receptor over-expression, we consider the following normalized distribution of receptor concentration:

$$\rho(x, y) = \rho_A(x) = \begin{cases} 1 + \Delta_\ell > 1 & (0 \le x < x_\ell) \\ 1 & (x_\ell < x < x_g) \\ 1 + \Delta_g > 1 & (x_g < x \le x_{\max}) \end{cases} . \tag{75}$$

For this $\rho(x, y)$, we have instead of (63)

$$\frac{1}{x_{\max}} J_A(\bar{s}_0) \equiv \left[\left\{1 + \delta_\ell \Delta_\ell + (1 - \delta_g)\Delta_g\right\} I_o(\bar{s}_0)\right]_{\bar{s}_0 = \varsigma_A}, \qquad \delta_k = \frac{x_k}{x_{\max}} < 1 \tag{76}$$

where ς_A is the solution of

$$I_o(\varsigma_A) = \frac{\frac{1}{4}}{1 + \Delta_\ell \delta_\ell + \Delta_g(1 - \delta_g)}, \tag{77}$$

or

$$\frac{16}{B_m(\zeta_A)}\tan^{-1}\left(\frac{1}{B_m(\zeta_A)}\right)+\frac{16}{B_p(\zeta_A)}\tanh^{-1}\left(\frac{1}{B_p(\zeta_A)}\right)$$
$$=\frac{\sigma_s v_L^*}{2[1+\Delta_\ell\delta_\ell+\Delta_g(1-\delta_g)]} \tag{78}$$

with B_m and B_p given in (59).

PROPOSITION 9. $\varsigma_A \equiv [\bar{s}_0]_{\rho=\rho_A} > [\bar{s}_0]_{\rho=\rho_o} \equiv \varsigma_0$.

Proof: This follows from the fact that the right-hand side of (77) is less than $\frac{1}{2}$ and I_o is a monotone decreasing function of $\bar{s}_0$ by Lemma 2. ■

5.2. Signaling receptor concentration

We now compare the signaling *Dpp* for the normal case of a uniformly distributed receptor concentration with one that is over-expressed at the two ends of the anterior–posterior axis, particularly the interval $x_\ell < x < x_g$ where the latter is not over-expressed.

For the uniformly distributed case, we have $[LR]_{\rho(x)=1}/\eta\bar{R}_0$ is given by (70) as before. For $\rho(x) = \rho_A(x)$, we have for the range $x_\ell < x < x_g$,

$$\frac{1}{\eta\bar{R}_0}[LR]_{\rho_A(x)} \sim \left[\frac{1}{\eta+s_0(y;\bar{s}_0)}\right]_{\bar{s}_0=\varsigma_A}$$
$$=\begin{cases}\left[\eta+\varsigma_A+\frac{1}{8}(y+2y^2)\right]^{-1} & (y<0)\\ \left[\eta+\varsigma_A+\frac{1}{8}(y-2y^2)\right]^{-1} & (y>0)\end{cases}$$
$$<\left[\frac{1}{\eta+s_0(y;\bar{s}_0)}\right]_{\bar{s}_0=\varsigma_0} \sim \frac{1}{\eta\bar{R}_0}[LR]_{\rho(x)=1} \tag{79}$$

where the inequality is a consequence of Proposition 9. The implication of (79) is summarized in the following proposition:

PROPOSITION 10. *At low receptor occupation and the out asymptotic solution applies, over-expressing Dpp receptors tkv at both end of the anterior–posterior*

axis reduces PMad activation in cells in the region $X_\ell < X < X_g$ outside the location with ectopic receptors.

For the intervals where *tkv* is over-expressed, the situation is again more complicated. In the range $0 < x < x_\ell$, we have

$$\frac{1}{\eta \bar{R}_0}[L\,R]_{\rho_A(x)} \sim \left[\frac{1+\Delta_\ell}{\eta + s_0(y;\bar{s}_0)}\right]_{\bar{s}_0=\varsigma_A} = \begin{cases} (1+\Delta_\ell)/\left[\eta + \varsigma_A + \dfrac{1}{8}(y+2y^2)\right] & (y<0) \\ (1+\Delta_\ell)/\left[\eta + \varsigma_A + \dfrac{1}{8}(y-2y^2)\right] & (y>0) \end{cases}. \tag{80}$$

The comparison with the corresponding concentration for a uniform receptor distribution now depends on the magnitude of Δ_ℓ. In particular, we have

PROPOSITION 11. *At low receptor occupation and the out asymptotic solution applies, over-expressing Dpp receptors tkv at both ends of the anterior–posterior axis by a sufficiently large concentration at the anterior end so that*

$$1 + \Delta_\ell > \frac{\eta + \varsigma_A - \dfrac{1}{16}}{\eta + \varsigma_0 - \dfrac{1}{16}} \tag{81}$$

elevates PMad activation in the interval $0 < x < x_\ell$ while the opposite is true if the inequality in (81) is reversed, at least in a region contiguous to the dorsal midline. A corresponding result applies to the posterior end.

5.3. Numerical results for the illustrative example

To provide numerical evidence in support of a depressed signaling gradient expression for an ectopic receptor distribution of the type $R_A(X)$ defined in (7), we consider such a receptor distribution with $\Delta_\ell = \Delta_g = 0.02$ cm. Given the symmetry of $R_A(X)$, a similar symmetry expected of the corresponding $[LR]$ expression is confirmed by the two-dimensional plot of its steady state in Figure 7 for $\bar{V}_L = 0.25 \times 10^{-3}\,\mu$M/s and $\bar{V}_S = 0.6\,\mu$M/s and the corresponding one-dimensional plot for its graph along the dorsal midline in Figure 8. Hence, we can limit our discussion to the steady-state behavior for the anterior half of the embryo (as we did in reporting the numerical results shown in Tables 5 and 6).

From the numerical results for the case $\bar{V}_L = 0.25 \times 10^{-3}\,\mu$M/s reported in Table 5, we see a good qualitative agreement between the numerical simulation results for $\bar{V}_S = 0.6\,\mu$M/s and the asymptotic results. As shown in Figure 8, the numerical solution for $[LR]$ along the dorsal midline for $\bar{V}_S = 0.6\,\mu$M/s is nearly uniform within the three subinterval $[0,\ X_\ell)$, $(X_\ell,\ X_g)$, and $(X_g,$

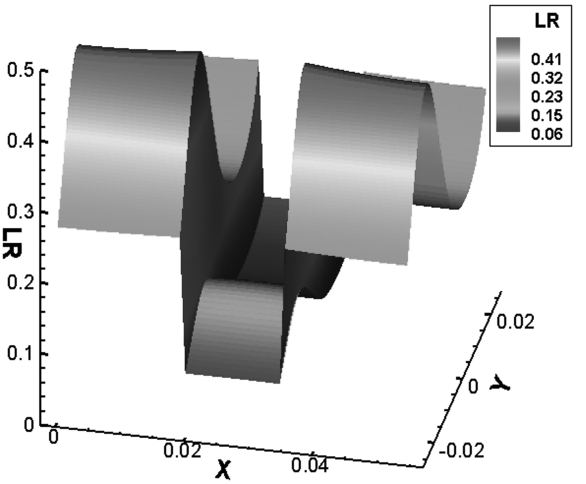

Figure 7. Two-dimensional plot of the [LR] distribution in μM for the fixed receptor expression $R_A(X)$ (with the same ectopic expression in $0 \leq X < X_\ell = 0.02\,\text{cm}$ and $X_g = 0.035\,\text{cm} < X \leq X_{\max}$) for $\bar{V}_L = 2.5 \times 10^{-4}\,\mu\text{M/s}$ and $\bar{V}_S = 0.6\,\mu\text{M/s}$.

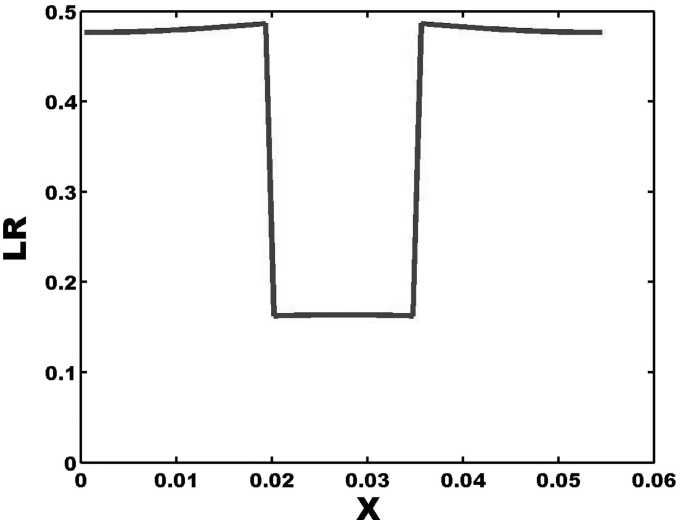

Figure 8. Distribution of [LR] in the anterior–posterior direction at the dorsal midline for the fixed receptor expression $R_A(X)$ (with the same ectopic expression in $0 \leq X < X_\ell = 0.02\,\text{cm}$ and $X_g = 0.035\,\text{cm} < X \leq X_{\max}$) for $\bar{V}_L = 2.5 \times 10^{-4}\,\mu\text{M/s}$ and $\bar{V}_S = 0.6\,\mu\text{M/s}$.

$X_{\max}$]. This is consistent with the prediction by the asymptotic steady-state solution. Furthermore, the trend of [LR] is toward the asymptotic solution as $\bar{V}_S$ increases from $10^{-3}\,\mu\text{M/s}$.

For the higher *Dpp* synthesis rate $\bar{V}_L = 10^{-3}\,\mu\text{M/s}$. the agreement between the numerical and asymptotic solution is also good but in a different way. With

Table 5
$[LR]$ at Dorsal Midline in μM

$(\bar{V}_L = 0.25 \times 10^{-3}\,\mu\text{M/s}, \delta_\ell = \delta_g = 4/11)$					
$\bar{V}_S$	δ_ℓ	$[LR]_{x=0}$	$[LR]_{x=x_\ell-}$	$[LR]_{x_\ell+}$	$[LR]_{x=x_{\max}}$
$10^{-3}\,\mu$M/s	0	0.5406..	0.5406..	0.5406..	0.5406..
	4/11	0.5134..	0.7741..	0.3572..	0.5134..
$8\times10^{-2}\,\mu$M/s	0	0.6314..	0.6314..	0.6314..	0.6314..
	4/11	0.4824..	0.5462..	0.1849..	0.4824..
$6\times10^{-1}\,\mu$M/s	0	0.6241..	0.6241..	0.6241..	0.6241..
	4/11	0.4686..	0.4778..	0.1597..	0.4686..
$\infty\ \mu$M/s	0	0.6239..	0.6239..	0.6239..	0.6239..
	4/11	0.3570..	0.3570..	0.1190..	0.3570..

Table 6
$[LR]$ at Dorsal Midline

$(\bar{V}_L = 10^{-3}\,\mu\text{M/s}, \delta_\ell = \delta_g = 4/11)$					
$\bar{V}_S$	δ_ℓ	$[LR]_{x=0}$	$[LR]_{x=x_\ell-}$	$[LR]_{x_\ell+}$	$[LR]_{x=x_{\max}}$
$10^{-3}\,\mu$M/s	0	0.5406..	0.5406..	0.5406..	0.5406..
	4/11	0.5126..	0.7452..	0.3530..	0.5426..
$8\times10^{-2}\,\mu$M/s	0	0.6314..	0.6314..	0.6314..	0.6314..
	4/11	2.9821..	5.6463..	2.0882..	2.9821..
$6\times10^{-1}\,\mu$M/s	0	0.6241..	0.6241..	0.6241..	0.6241..
	4/11	3.7793..	4.9604..	1.7012..	3.7793..
∞	0	0.6239..	0.6239..	0.6239..	0.6239..
	4/11	3.0710..	3.0710..	1.0237..	3.0710..

more *Dpp* available, the same *Sog* synthesis rate $\bar{V}_S = 0.6\,\mu$M/s proportionally less *Dpp* is transported toward the anterior end of the embryo, especially near the anterior vertex. Consequently, there is a more pronounced nonuniformity in each of the three subintervals (qualitatively similar to the distribution for $R_h(X)$), decreasing in magnitude from X_ℓ to 0 (and by symmetry from X_g to $X_{\max}$). Because of less transport, more *Dpp* molecules are degraded, especially in the waist region of the embryo $X_\ell < X < X_g$ resulting in a lower $[LR]$ concentration than that for $\bar{V}_L = 0.25 \times 10^{-3}\,\mu$M/s. On the other

hand, the discrepancy between numerical and asymptotic solution for [*LR*] is substantially less than those of Table 5 for the lower Dpp synthesis rate case.

6. Asymptotic behavior for $\bar{V}_L \gg \bar{V}_S$

For the biologically less realistic case of $\bar{V}_S/\bar{V}_L = 1/\varepsilon \ll 1$, the structure of the BVP admits a regular perturbation solution in powers of $1/\varepsilon$. The governing equations for the leading term solution, $\{a^0, \ldots, s^0\}$, corresponds to setting $1/\varepsilon = 0$ in (34)–(36) to get

$$\mu_L^{-2}\nabla^2 a^0 - \frac{\rho a^0}{1+\beta_L a^0} + H(-y) = 0, \tag{82}$$

$$(f_S + g_S)^{-1}\nabla^2 c^0 + \left(\nu_L^* a^0 s^0 - c^0\right) = 0, \tag{83}$$

$$\nabla^2 s^0 - \left(\nu_L^* a^0 s^0 - c^0\right) - \sigma_S c^0 + H(y) = 0. \tag{84}$$

Note that the form of equations (35) and (36) is not changed by setting $1/\varepsilon = 0$; nor is the equation (37) giving $b(x, y; \varepsilon)$ in terms $a(x, y; \varepsilon)$:

$$b^0(x, y) = \frac{\rho(x)\beta_L a^0(x, y)}{1+\beta_L a^0(x, y)}. \tag{85}$$

More importantly, (82) is an equation for $a^0(x, y)$ alone and, augmented by the homogeneous Neumann condition along the edges of the rectangular domain, may be solved separately.

PROPOSITION 12. *For $\beta_L < 1$, a unique nonnegative solution of the BVP for a^0 exists with*

$$0 \le a^0(x, y) \le a_u \tag{86}$$

where the constant a_u is given by

$$a_u = \frac{1}{1-\beta_L}.$$

Proof: Evidently, $a_\ell = 0$ is a lower solution for the problem. On the other hand, we have

$$\begin{aligned} &-\mu_L^{-2}\nabla^2 a_u + \frac{\rho(x)a_u}{1+\beta_L a_u} - H(-y) \\ &\quad = \frac{[\rho(x)-1]a_u}{1+\beta_L a_u} + 1 - H(-y) = \rho(x) - 1 + H(y) > 0 \end{aligned}$$

given $\rho \geq 1$. With $\partial a_u/\partial n = 0$, a_u is an upper solution for the BVP. Hence, a solution of the BVP problem exists and is bounded above and below as in (86) [28–30]. Uniqueness is proved as in [8]. ■

Having the piecewise C^2 solution for $a^0(x, y)$, equations (83) and (84) together with the relevant homogeneous Neumann conditions may be solved for $c^0(x, y)$ and $s^0(x, y)$. Note that the two PDE (83) and (84) are linear in the two unknowns. Actual solutions may be obtained by methods similar to those used in [5, 18]. However, for the purpose of delineating the effects of locally over-expressed *tkv* on cell signaling, we need only the solution of (82) with which we can calculate [*LR*] from (85). The numerical solution for the BVP for $a^0(x, y)$ is straightforward. Given that μ_L^{-2} is typically small compared to unity, we note also the singular perturbation structure of (82) with respect to the parameter μ_L so that asymptotic solution for large μ_L is also possible. Sample solutions have been obtained for typical sets of parameter values used in [8, 18, 31]. The results on depression of *Dpp* signaling by localized over-expression of receptors are qualitatively different from that stated in Proposition 6 for $\rho(x) = \rho_h(x)$ regarding the abrupt depression of the bound morphogen concentration posterior to the region of the elevated receptor concentration.

7. Conclusion

When the receptor expression is ectopic in the anterior end of an *Drosophila* embryo, our study of a simple mathematical model based on the essential biological processes for morphogen gradients in *Drosophila* embryos identified in [7, 13] shows that a depression of the signaling *Dpp-tkv* concentration in the posterior does occur under suitable conditions. At the same time, a lack of *Dpp-tkv* concentration depression as noted in the work of Wang and Ferguson [16] is now seen to be possible as well for a number of reasons including:

- Sufficiently high *Dpp* and *Sog* synthesis rates that saturate the fixed receptor expression throughout the posterior portion of the embryo (see the case $\bar{V}_L = 10^{-3}\,\mu$M/s and $\bar{V}_S = 0.6\,\mu$M/s in Table 4).
- A sufficiently low *Sog* synthesis rate that does not shuttle much if any *Dpp* to the anterior region except in a narrow layer adjacent to the location of receptor expression discontinuity as seen from the case of $\bar{V}_S = 10^{-3}\,\mu$M/s in both Tables 2 and 4. (Not shown by the tables is the substantial depression of [*LR*] in each case is confined to a narrow region with the width of the region becoming narrower as $\bar{V}_L$ increases.)
- A relatively low elevation of the receptor expression in the anterior region which allows enough *Dpp* for binding in the posterior region (except for a narrow phenomenon near X_h) as shown in Table 2 for $\bar{V}_S = 10^{-3}\,\mu$M/s.

It is also seen from Table (2) (and the graphs for [*LR*] for the case of $\bar{V}_L = 2.5 \times 10^{-4}\,\mu$M/s not shown herein) that the depression in the posterior region (and the elevation in the anterior region) becomes more uniform in X with increasing $\bar{V}_S$. This suggests that the partial depression over a small subinterval of the posterior end near the location of receptor expression discontinuity for the case of $R_h(X)$ may be the consequences of three different phenomena:

- A very low *Sog* synthesis rate $\bar{V}_S$ that transports to the nearby anterior region only the *Dpp* and *Dpp-Sog* in a narrow layer adjacent to the location X_h of the discontinuity in $R_h(X)$.
- Intermediate Sog synthesis rates that manage to shuttle sufficient *Dpp* and *Dpp-Sog* away from a finite interval (X_h, X_g) in the posterior region to the anterior region with X_g substantially smaller than $X_{\max}$.
- The receptor expression is elevated at both end (qualitatively similar to the results for $R_A(X)$) leading to an [*LR*] gradient elevated at both ends and depressed in region of normal receptor expression in between (see Tables 5 and 6).

The results from our simple mathematical model also offer new insight not previously observed. One important result of this category is the variability of the elevation in [*LR*] in the region of ectopic receptor expression. From the asymptotic analysis of Sections 3 and 5, we now know that [*LR*] expression may be elevated, unchanged or even depressed depending on the combinations of the various rate parameter values. In particular, we have from Propositions 7 and 11 that

- An elevation of the receptor expression in the ectopic region not sufficiently high would result in no change or a depression (rather than an elevation) of signaling morphogen gradient [*LR*] in the anterior region if it does not meet the condition (such as (74) for $R_h(X)$ and (81) for $R_A(X)$) required for an elevated [*LR*] expression.

It should be noted that some of the results obtained by our asymptotic analysis and numerical simulations are consequence of our simplifying assumption of a fixed receptor expression throughout the embryo which may or may not persist should we allow for receptor synthesis and renewal. It should persist if the receptor-mediated Dpp degradation rate constant is the same as the degradation rate constant of unoccupied receptors. Research results for the more realistic model allowing for receptor renewal will be reported elsewhere. Meanwhile, the results for the fixed receptor expression model reported herein should serve much more than a proof of concept on how we may address the question whether there should be a depression of BMP signaling posterior to the anterior region of ectopic receptor expression and how it should depend on the level of *Sog* synthesis rate and other rate constants.

Acknowledgments

The research was supported in part by NIH grants P50-GM076516, R01GM067247, and R01GM075309. The two NIH R01 grants were awarded through the Joint NSF/NIGMS Initiative to Support Research in the Area of Mathematical Biology. The research of Y.-T. Zhang at the University of Notre Dame was partially supported by Oak Ridge Associated Universities (ORAU) Ralph E. Powe Junior Faculty Enhancement Award and by NSF research grant DMS-0810413.

References

1. A. A. Teleman, M. Strigini, and S. M. Cohen, Shaping morphogen gradients, *Cell* 105:559–562 (2001).
2. L. Wolpert, R. Beddington, J. Brockes, T. Jessel, P. Lawrence, and E. Meyerowitz, *Principles of Development* (2nd ed.), Oxford University Press, New York, 2002.
3. E. V. Entchev, A. Schwabedissen, and M. Gonzalez-Gaitan, Gradient formation of the TGSF-beta homolog Dpp, *Cell* 103:981–991 (2000).
4. A. A. Teleman and S. M. Cohen, Dpp gradient formation in the *Drosophila* wing imaginal disc, *Cell* 103:971–980 (2000).
5. A. Eldar, R. Dorfman, D. Weiss, H. Ashe, B. Z. Silo, and N. Barkai, Robustness of MmP morphogen gradient in *Drosophila* embryonic patterning, *Nature* 419:304–308 (2002).
6. J. B. Gurdon and P. Y. Bourillot, Morphogen gradient interpretation, *Nature* 413:797–803 (2001).
7. A. D. Lander, Q. Nie, and F. Y. M. Wan, Do Morphogen Gradients Arise by Diffusion? *Dev. Cell* 2:785–796 (2002).
8. A. D. Lander, Q. Nie, and F. Y. M. Wan, Spatially distributed morphogen production and morphogen gradient formation, *Math. Biosci. Eng. (MBE)* 2:239–262 (2005).
9. H. L. Ashe and M. Levine, Local inhibition and long-range enhancement of Dpp signal transduction by Sog, *Nature* 398:427–431 (1999).
10. E. Bier, A unity of opposites, *Nature* 398:375–376 (1999).
11. M. Oelgeschlager, J. Larrain, D. Geissert, and E. M. Roberts, The evolutionarily conserved bmp-binding protei twised gastrulation promotes bmp signalling, *Nature* 405:757–762 (2000).
12. J. J. Ross, O. Shimmi, P. Vilmos, A. Petryk, H. Kim, K. Gaudenz, S. Hermanson, S. C. Ekker, M. B. O'Connor, and J. L. Marsh, Twisted gastrulation is a conserved extracellular BMP antagonist, *Nature* 410:479–483 (2001).
13. C. M. Mizutani, Q. Nie, F. Y. M. Wan, Y.-T. Zhang, P. Vilmos, E. Bier, J. L. Marsh, and A. D. Lander, Formation of the BMP activity gradient in the *Drosophila* embryo, *Dev. Cell* 8:915–924 (2005) (with Supplement).
14. J. Kao, Q. Nie, A. Teng, F. Y. M. Wan, A. D. Lander, and J. L. Marsh, Can morphogen activity be enhanced by its inhibitors? in *Proceedings of the 2nd MIT Conference on Computer Mechanics* (K. J. Bathe, Ed.), Elsevier Science Ltd, Vol. 2, pp. 1729–1734, 2003.
15. Y. Lou, Q. Nie, and F. Y. M. Wan, Effects of Sog on Dpp-receptor binding, *SIAM J. Appl. Math.* 65:1748–1771 (2005).

16. Y.-C. Wang and E. L. Ferguson, Spatial bistability of Dpp-receptor interactions during *Drosophila* dorsal–ventral patterning, *Nature* 434:229–234 (2005).
17. D. Iron, A. Syed, H. Theisen, T. Lukacsovich, M. Naghibi, J. L. Marsh, F. Y. M. Wan, and Q. Nie, The role of feedback in the formation of morphogen territories, *Math. Biosci. Eng. (MBE)* 5(2):277–298 (2008).
18. B. Vargas, Leaky boundaries and morphogen gradient formation, Ph.D. Dissertation, University of California, Irvine, December 2007.
19. Y. Lou, Q. Nie, and F. Y. M. Wan, Nonlinear eigenvalue problems in the stability analysis of morphogen gradients, *Stud. Appl. Math.* 113:183–215 (2004).
20. A. D. Lander, Q. Nie, and F. Y. M. Wan, Internalization and end flux in morphogen gradient formation, *J. Comp. Appl. Math*. 232–251 (2006).
21. F. C. Crick, Diffusion in embryogenesis, *Nature* 225:40–42 (1970).
22. M. Kerszberg and L. Wolpert, Mechanisms for positional signalling by morphogen transport: A theoretical study, *J. Theor. Biol.* 191:103–114 (1998).
23. G. Marques, M. Musacchio, M. J. Shimell, K. Wunnenberg-Stapleton, K. W. Cho, and M. B. O'Connor, Production of a DPP activity gradient in the early *Drosophila* embryo through the opposing actions of the SOG and TLD proteins, *Cell* 91:417–426 (1997).
24. S. Piccolo, E. Agiusa, B. Lu, S. Goodman, L. Dale, and E. De Roberts, Cleavage of chordin by xolloid metalloprotease suggests a role for proteolytic processing in the regulation of spemann organizer activitiy, *Cell* 91:407–416 (1997).
25. A. D. Lander, Q. Nie, and F. Y. M. Wan, Membrane associated non-recptors and morphogen gradients, *Bull. Math. Bio.* 69:33–54 (2007).
26. B. Gustafsson, H.-O. Kreiss, and J. Oliger, *Time Dependent Problems and Difference Methods*, Wiley, New York, 1995.
27. J. Stoer and R. Bulirsch, *Introduction to Numerical Analysis*, Springer-Verlag, New York, 1993.
28. H. Amann, On the existence of positive solutions of nonlinear boundary value problems, *Indiana Univ. Math. J.* 21:125–146 (1971).
29. D. H. Sattinger, Monotone methods in nonlinear elliptic and parabolic boundary value problems, *Indiana Univ. Math. J.* 21:981–1000 (1972).
30. J. Smoller, *Shock Waves and Reaction-Diffusion Equations*, Springer-Verlag, New York, 1982.
31. Q. Nie, F. Y. M. Wan, Y.-T. Zhang and X.-F. Liu, Compact integration factor methods in high spatial dimensions, *J. Comp. Phys.* 227:5238–5255 (2008).

University of California, Irvine

(Received September 16, 2008)